Microtubules control Buc Phase separation and Balbiani body condensation in zebrafish oocyte polarity

Rachael Deis[1,2] and Yaniv M. Elkouby[1,2] *

[1]Department of Developmental Biology and Cancer Research, The Hebrew University of Jerusalem Faculty of Medicine, Ein-Kerem Campus, Jerusalem, Israel 9112102

[2]Institute for Medical Research – Israel-Canada (IMRIC), Ein-Kerem Campus, Jerusalem, Israel 9112102

*Corresponding author. Email: yaniv.elkouby@mail.huji.ac.il

Abstract

Molecular condensates provide new paradigms in biology, but their cellular regulation is unclear. Condensates undergo phase separation, decreasing their solubility and compartmentalizing their content. In vertebrate oocytes, RNA-protein (RNP) granules form condensates by phase separation, but the underlying mechanisms are unknown. RNP granules localize to the Balbiani body (Bb), a conserved membraneless organelle, that establishes oocyte polarity. Bb loss results in symmetrical eggs and embryonic lethality. Bb granules aggregate around the centrosome in a nuclear cleft, prior to assembling the mature structure. The Bucky ball (Buc) protein nucleates Bb granules and is essential for Bb formation. Howe ver, the dynamics, mechanisms, and regulation of Bb granule nucleation are unclear. While the mature Bb structure was shown to be a rigid, amyloid-like, phase-separated structure in *Xenopus*, the early phase separation dynamics prior to maturation are completely unknown. Here, by live, genetic, super-resolution microscopy, and FRAP analyses in zebrafish ovaries, we establish that Buc phase-separates Bb granules and that microtubules play multiple stepwise roles in controlling Buc phase separation and Bb formation specifically at the early nuclear cleft stages. We show that Buc first phase-separates into dynamic liquid droplet-like granules that fuse to form the main Bb aggregate. We demonstrate that early aggregated Buc exhibited dynamic turnover and that this turnover requires dynein-mediated trafficking of Buc on a transient lattice of microtubules that we identified. At later stages, microtubules encapsulated the Bb, indicating a structural role. Thus, microtubules organize multiple steps in Bb condensation. Moreover, in the mature Bb, Buc was stable and required for Bb amyloid formation, finalizing Bb condensation. We found for the first time by live imaging, ThT-positive presumptive amyloid ß-sheets in the mature zebrafish Bb, that we re absent in *buc*$^{-/-}$ oocytes. Thus, providing the first genetic evidence for Buc dependent formation of presumptive amyloid fibrils in the Bb. Molecular condensation is often viewe d as a self-assembly process. Here, we propose a novel paradigm for the cellular control over condensation mechanisms by microtubules in development. The regulation of Bb assembly and disassembly in the context of phase separation allows studying these mechanisms in physiological conditions, advancing their understanding in neurodegenerative disease and female reproduction.

Introduction

A major question in biology is how the densely packed cytoplasm of a cell is organized to enable complex biochemical reactions in space and time. Eukaryotic cells achieve spatiotemporal control by producing a multitude of subcellular compartments to regulate the localization of reaction components. In general, compartments consist of two important properties: **(1)** a boundary that separates it from its surroundings, and **(2)** components that experience free diffusion inside, so that chemical reactions can take place (Hyman et al., 2014). Classic subcellular compartments and organelles are surrounded by a bi-lipid membrane, such as mitochondria. Bi-lipid membranes provide physical separation from the cell's cytoplasm and are regulated through specialized membrane transport machineries. Howe ver, many other cellular compartments are not bound by membranes, yet remain distinct from the surrounding cytoplasm. While membraneless compartments have been observed for two centuries, how they maintain their structure and concentrate molecules for regulating their function was unknown (Banani et al., 2017).

In recent years, many membraneless compartments that are involved in a wide range of cellular processes have been identified, including RNA-protein granules such as nucleoli, Cajal bodies and nuclear speckles in the nucleus, as we ll as stress granules, processing bodies (P-bodies) and germ granules in the cytoplasm (Banani et al., 2017; Boeynaems et al., 2018; Dodson & Kennedy, 2020; Hyman et al., 2014). Non-membrane-bound compartments are extremely diverse in their physical properties and have been referred to by various names over the years, including membraneless organelles, granules, aggregates, nuclear bodies and membrane puncta (Banani et al., 2017). These subcellular compartments all share the ability to concentrate molecules by exploiting a mechanism known from physical sciences, called phase separation (see chapter **1.1.1**), which essentially decreases their solubility in a solution. Hence, the name "biomolecular condensates" was recently adopted by the field (Banani et al., 2017; Dodson & Kennedy, 2020). Biomolecular condensates have the ability to concentrate nucleic acids and proteins at specific cellular sites without the use of physical barriers such as a bi-lipid membrane (Banani et al., 2017). Many key protein complexes such as the nucleoporins in the vicinity of nuclear pore complexes (NPC) (Frey & Gorlich, 2007), the peri-centriolar material of the centrosome (Mahen & Venkitaraman, 2012), and synaptonemal complexes that connect homolog chromosomes in meiosis (Rog et al., 2017; So et al., 2021) have been recently described as biomolecular condensates. Understanding how their regulation and organization contributes to the development of multicellular organisms as we ll as how their dysregulation and metastability can lead to protein aggregation diseases has created a new field in cell biology.

It has become clear in recent literature that biomolecular condensates form via liquid-liquid phase separation (LLPS), explaining their diverse material properties and complex subcellular organization. LLPS explains the presence of a phase boundary betwe en the less soluble bio-condensate and their more soluble surroundings. This results in the creation of two distinct liquid phases, similar to how oil separates from vinegar in vinaigrette (Dodson & Kennedy, 2020; Hyman et al., 2014). Molecules will phase-separate once they reach their solubility limit or threshold concentration in solution (Hyman et al., 2014). In this model, instead of entropy driving the system to a mixed state, the spontaneous separation into two phases (i.e. oil and vinegar) is driven by the interactions betwe en the molecules themselves which favor the formation of liquid-like droplets or condensates in the solution (Banani et al., 2017; Hyman et al., 2014). That is to say that these types of molecules are attracted to each other causing the "demixed" state to have lowe r energy and be favored over the mixed state (Hyman et al., 2014). For example, oil-oil interactions are favored over oil-vinegar interactions, ultimately allowing for liquid-like droplets to self-assemble within another liquid. Thus, the phase separated state has the minimum free energy (equilibrium) that allows cells to maintain concentration differences without constant input of energy (Banani et al., 2017; Boeynaems et al., 2018; Hyman et al., 2014).

A driving force underlying the assembly of these liquid condensates within cells are multivalent molecules such as protein-protein and protein-RNA interactions (Shin & Brangwynne, 2017; Zhang et al., 2015). Specifically, proteins composed of multiple modular interaction domains and repeats of the same type of domain provide multiple we akly adhesive sequence elements that decrease the solubility of molecules, thus promoting their phase separation (Banani et al., 2017; Frey et al., 2006; Hulsman et al., 2012; Shin & Brangwynne, 2017). These include regulatory proteins in many signal transduction pathways, such as growth factor receptor-bound protein 2 (Grb2), that contain repeats of the SH3 domain that binds to proline-rich motifs (PRMs) (Shin & Brangwynne, 2017). Proteins that contain intrinsically disordered regions (IDRs) (also known as intrinsically disorder proteins, IDPs) are also key for driving liquid-liquid phase separation (Shin & Brangwynne, 2017). While IDPs/IDRs lack hydrophobic residues that drive higher-order folding, they are typically enriched in polar and charged amino acids such as glycine (G), serine (S), glutamine (Q), proline (P), glutamic acid (E), lysine (K), and arginine (R) (Shin & Brangwynne, 2017). Their sequences found in condensates also tend to be interspersed with aromatic residues such as tyrosine (Y) and phenylalanine (F) (Shin & Brangwynne, 2017). Indeed, numerous in vitro and in vivo studies have shown that IDR sequences drive phase separation. The amyotrophic lateral sclerosis (ALS)-related and stress granule-associated proteins hnRNPA1, FUS and TDP43, as we ll as the mitotic spindle protein BuGZ and cell-cycle protein Whi3 are just a few examples (Shin &

Brangwynne, 2017). While IDRs can drive phase separation alone, it is we ll established that RNA can further promote this process by lowe ring the saturation concentration needed to trigger phase separation (Dodson& Kennedy, 2020; Shin & Brangwynne, 2017).

While IDRs drive phase separation, their heterotypic interactions with RNA are also extremely important. It was shown that IDPs/IDRs are key players in the formation of RNA-protein (RNP) granules and contain various RNA-binding domains including RRM, RGG repeats, and enzymatic domains (Boke et al., 2016; Brangwynne et al., 2009; Roovers et al., 2018; Shin & Brangwynne, 2017). RNP complexes are we ll studied molecular condensates. These include P-bodies (Luo et al., 2018) and stress granules (Buchan & Parker 2009, Decker & Parker 2012; Hanson & Mair, 2013) in somatic cells, as we ll as RNP granules in the germline, such as P granules in *Caenorhabditis elegans* (*C.elegans*) (Aoki et al., 2021; Brangwynne et al., 2009; Folkmann et al., 2021; Wang et al., 2014), polar granules in *Drosophila* (Jeske et al., 2015; Kistler et al., 2018; Trcek et al., 2015), and piRNA granules and Balbiani bodies in vertebrates (Elkouby et al., 2016; Elkouby & Mullins, 2017a; Kloc et al., 2004; Nott et al., 2015; Schisa, 2012; Tian et al., 2020). The most extensive documentation and categorization of IDP function in RNP granules exists in the context of P granule formation in *C.elegans* (Putnam et al., 2019; Seydoux, 2018; Spike et al., 2008; Marnik et al., 2019). Some of these include proteins rich in serine (MEG-3, MEG-4 and DEPS-1), arginine/glycine-rich (RGG/RG) RNA binding domains (PGL-1, PGL-3 and LAF-1) and multiple FG-repeat proteins like the RNA helicase GLH-1(Putnam et al., 2019; Seydoux, 2018; Spike et al., 2008; Marnik et al., 2019). Interactions betwe en IDRs in these proteins induce the formation of RNP granules by decreasing their solubility in several general steps: **(1)** Increasing the local concentration of the IDR protein above a threshold to trigger the initial phase separation; **(2)** These higher local concentrations then bring together IDRs, increasing the affinity betwe en we ak interacting molecules and modify the charge and physical properties of the complex; **(3)** Interacting IDRs further seed and nucleate more IDR proteins in the complex, further decreasing its solubility and promoting the formation of larger RNP complexes (Banani et al., 2017; Boeynaems et al., 2018; Guo & Shorter 2015; Shin & Brangwynne, 2017). Thus, IDRs are an important driving force for phase separation by providing multiple points of contact betwe en molecules, resulting in less soluble and increasingly adhesive structures.

Protein-protein and protein-RNA phase transitions and interactions exhibit different material states and dynamics. It has been proposed that phase separation within cells results in a variety of

condensates that can be placed on a scale from more liquid-like to solid-like, in different systems. These include liquid-like droplets of RNA-protein granules, hydrogels within the nuclear pore complexes, and solid-like protein assembly held together by strong amyloid ß-sheets such as the Balbiani body of oocytes (Boeynaems et al., 2018; Boke et al., 2016; Hyman et al., 2014). The most dynamic liquid-like condensates are highly sensitive to shifts in temperature and pH while the solid, less dynamic condensates tend to be more stable and resistant to changes in environmental factors (Boeynaems et al., 2018; Boke et al., 2016; Dodson & Kennedy, 2020; Folkmann et al., 2021; Hyman et al., 2014). Droplets formed by IDR containing proteins are particularly interesting in this regard. IDRs like FUS and hnRNPA1 initially exhibit liquid-like properties and rapidly exchanging molecules with their environment (Banani et al., 2017; Boeynaems et al., 2018). Yet over time, they start behaving like solids and cease to exchange molecules with their surroundings. This process has been referred to as hardening or maturation and is known to occur both in vitro and in vivo (Banani et al., 2017; Boeynaems et al., 2018). Moreover, IDRs are prone to fold into stable amyloid structures that contain insoluble ß-sheets and have roles in neurogenerative disorders such as Parkinson Disease and Alzheimer Disease (Banani et al., 2017; Boke and Mitchison, 2016; Scialò et al., 2019 Howe ver, little is known about how these IDRs transition from liquid-like to maturation and the physical properties associated with the different material states that can be essential for development or detrimental in the context of disease.

Moreover, the role of amyloid-like structures in physiological processes such as gametogenesis is extremely understudied. The fact that the soluble versus condensed states of these complexes are specifically required in distinct developmental and physiological contexts strongly suggests that the transition betwe en these states is subjected to tight cellular regulation (Banani et al., 2017; Boeynaems et al., 2018; Dodson & Kennedy, 2020; Folkmann et al., 2021; Hyman et al., 2014). For example, RNA binding proteins often contain IDRs adjacent to their RNA binding domains, such that initial RNA binding increases the IDR concentrations over the required threshold for their interactions to trigger phase separation (Folkmann et al., 2021; Gross-Thebing & Raz, 2020; Guo & Shorter, 2015; Luo et al., 2018). RNA binding in such cases can be regulated to control the rate and extent of phase separation of their corresponding RNP granule (Folkmann et al., 2021; Gross-Thebing & Raz, 2020; Guo & Shorter, 2015; Luo et al., 2018). Recent work has revealed that RNA can also promote phase separation independently of IDRs (see chapter **1.1.1.**) (Shin & Brangwynne, 2017). Moreover, the ability of IDRs to interact and change the charge of their complex(es) can be modified by post-translational modifications (Folkmann et al., 2021; Gross-Thebing & Raz, 2020; Luo et al., 2018). For example, phosphorylation of the IDR protein MEG-3, which mediates P granule condensation in *C. elegans*

embryos, disrupts such interactions promoting the dissolved state of P granule components over their condensed form (Folkmann et al., 2021; Wang et al., 2014). Nevertheless, such reported regulatory mechanisms are sparse. The regulation of the recruitment of IDR proteins over their required threshold, their IDR interactions, as we ll as the regulatory proteins that control their rate and extent of condensation are largely unknown, especially in vertebrates.

In vertebrate oocytes, phase-separated RNP granules are found within a large membraneless organelle, called the Balbiani body (Bb) (Elkouby, 2017; Escobar-Aguirre et al., 2017a; Jamieson-Lucy & Mullins, 2019; Kloc et al., 2004). In addition to RNP granules, the Bb also contains cellular organelles, such as mitochondria, and is conserved in oocytes from insects to human (Boke et al., 2016; Cox & Spradling, 2003; De Smedt et al., 2000; Elkouby et al., 2016; Hertig, 1968; Kloc et al., 2004; Pepling et al., 2007). Widely in animals and plants, gamete polarization lays the foundations for early embryonic development. In most vertebrates, including zebrafish, the Bb is required for the establishment of the oocyte animal-vegetal (AV) axis (Elkouby, 2017; Escobar-Aguirre et al., 2017a; Jamieson-Lucy & Mullins, 2019). The Bb specifies the oocyte vegetal pole (Elkouby et al., 2016; Elkouby, 2017), which is key for embryonic development, harboring patterning factors that establish the global embryonic body axes and the germline lineage (Elkouby, 2017; Escobar-Aguirre et al., 2017a; Langdon & Mullins, 2011). The Bb forms adjacent to the nucleus and translocates to the oocyte cortex, where it dissociates and unloads its RNPs to specify the vegetal pole of the oocyte (Elkouby, 2017; Escobar-Aguirre et al., 2017b; Jamieson-Lucy & Mullins, 2019; Langdon & Mullins, 2011). Moreover, loss of the Bb results in radially symmetrical eggs and early embryonic lethality (Dosch et al., 2004; Marlow & Mullins 2008). Consistently with the importance of the Bb to oocyte development, in mice, where the oocyte is not polarized, the Bb is associated with oocyte quality control and proper primordial follicle formation (Lei & Spradling, 2016; Jamieson-Lucy & Mullins, 2019).

The Bb strcutre and function are best stuided in zebrafish (Elkouby et al., 2016; Elkouby 2017; Marlow & Mullins 2008; Roovers et al., 2018) and *Xenopus* (Boke et al., 2016; Boke and Mitchison 2017; Chang et al., 2004; Kloc et al., 2004; Yang et al., 2015). It has been shown in *Xenopus* that the mature Bb contains amyloid ß-sheets, exhibiting characteristics of a prion-like aggregates that are rigid and non-dynamic (Boke et al., 2016; Boke and Mitchison 2017). Prion-like aggregates are amyloid deposits that originally arise from the conformational transition of normally soluble proteins into highly ordered fibrillar aggregates (Henning et al., 2015; Krammer et al., 2009). This prion-like aggregation mechanism ultimately results in the transtion of proteins (such as IDPs) from an initial liquid-like soluble

state to a solid-like state through their capacity to seed the aggregation of homotypic native proteins and propagate their amyloid states in a prion-like manner (Henning et al., 2015; Krammer et al., 2009). The amyloid fibrils of these proteins are formed by nucleated polymerization, a process also shared by prions, and thus this process is refered to as prion-like formation or aggregation throughout this work (Henning et al., 2015; Krammer et al., 2009).

The mature *Xenopus* Bb is resistant to harsh conditions such as high salt and high temperatures and has a very low turnover rate with the cytoplasm as determined by fluorescence recovery after photobleaching (FRAP) experiments (Boke et al., 2016). First identified in zebrafish through maternal-effect genetic screens, the prion-like domain (PDL) containing protein Bucky ball (Buc) is the only known essential protein for Bb formation in any species (Dosch et al., 2004; Marlow & Mullins 2008). Prion-like domains are low complexity sequences found in RNA binding proteins and have recently been implicated in mediating gene regulation via liquid-phase transitions that drive RNP granule assembly by promoting protein aggregation (described above) (Henning et al., 2015). The prion-like domain of the Buc *Xenopus* ortholog, XVelo, was found to form SDS-resistant amyloid aggregates in vitro and was required for recruiting XVelo to the Bb in oocytes (Boke et al., 2016; Chang et al., 2004; Marlow & Mullins 2008). Swapping XVelo prion-like domain with that of Buc was fully functional in recruiting XVelo to the Bb, demonstrating the functional conservation of this domain (Boke et al., 2016). Buc was recently proposed to function equivalently to Oskar, which mediates phase separation of polar granules in *Drosophila* embryos, in forming RNP granules (Kistler et al., 2018).

Bb localization of specific RNAs, proteins, and mitochondria are directly demonstrated and its polarization roles are readily evident in the zebrafish oocyte (Dodson & Kennedy, 2020; Elkouby 2017; Elkouby et al., 2016; Elkouby & Mullins, 2017a; Escobar-Aguirre et al., 2017a). The early stages of Bb formation we re recently characterized in zebrafish oogenesis and there is evidence suggesting Buc has prion-like functions as we ll (Elkouby et al., 2016). ourlab previously established methodologies to analyze early oogenesis in the juvenile zebrafish ovary (Elkouby et al., 2016; Elkouby, 2017; Elkouby &Mullins, 2017b), including: **(1)** defining criteria for oocyte staging and characterizing ovarian post-embryonic development, **(2)** establishing protocols for ovarian quantitative imaging and live time-lapse analysis in vivo and in culture, and **(3)** developing a method to isolate stage specific oocytes for biochemical analysis, and generating a stage-specific oocyte transcriptomic data. Using these methods,ourlab traced Bb formation and oocyte polarity to the onset of meiotic differentiation in oocytes, when the oocyte undergoes symmetry breaking (Elkouby et al., 2016).

In symmetry breaking, Bb components, including Buc, first polarize and localize around the oocyte centrosome (Elkouby et al., 2016). After symmetry breaking, aggregated Bb granules nucleate around the centrosome in a specialized nuclear cleft to assemble the compact mature Bb (Elkouby et al., 2016) It was further suggested that microtubules play a role in early Buc localization to the nuclear cleft during initial symmetry breaking stages (Elkouby et al., 2016). Previous *buc*$^{-/-}$ analysis has revealed that Buc is required specifically for granule nucleation during Bb assembly in the early oocyte (Elkouby et al., 2016). Interestingly, *buc*$^{-/-}$ ovaries initially display normal early polarization in early cleft stages. It is only at later developmental stages that the Bb granules disperse radially around the nucleus and fail to form the mature Bb structure. In contrast, within the nuclear cleft of *wt* oocytes, the Bb gradually becomes more compact as it reaches maturation, while the nuclear envelop concomitantly rounds out. This developmental formation of the Bb is consistent with the phase separation process previously described, where local protein concentrations increase over time, generating compact granules that transition from liquid-like condensates to more gel-like aggregates that finally form a solid-like mature structure with an amyloid-like matrix.

Despite the importance and conservation of the Bb, little is known about its early formation, specifically regarding the aggregation mechanisms of the only known essential protein Buc. While the mature Bb structure was shown to be a rigid, amyloid-like, phase-separated structure in *Xenopus*, the early phase separation dynamics prior to maturation are completely unknown. How early Bb aggregates form and localize to the nuclear cleft, their phase separation dynamics, and their underlying regulatory mechanisms and factors are unclear. Until now, only two Buc binding proteins we re identified, Rbpms2a/b and the multi-Tudor domain-containing protein, Tdrd6a, both dispensable for Buc localization and/or Bb assembly (Kaufman et al., 2018; Roovers et al., 2018). Tdrd6a was shown to bond a tri-RG domain in Buc that is methylated to subsequently affect aggregation suggesting that Bb dynamics may be subject to regulation by post-translational modifications by Tdrd6a (Roovers et al., 2018). Howe ver, the loss of Tdrd6a only mildly affected Bb morphology, highlighting additional unknown regulation (Roovers et al., 2018). Post-translational modifications of intrinsically disordered proteins likely trigger a variety of effects on phase separation in germ cells (Roovers et al., 2018). Nevertheless, Buc localization dynamics and turnover, as we ll as its essential partner(s) and/or regulatory proteins in the early oocyte have yet to be identified.

Results

To account for all the properties of the Balbiani body mentioned above, we hypothesized that the early Bb granules initially assemble via liquid phase separation, but then gradually harden into a solid-like state by forming an amyloid-like matrix. We reasoned that Buc aggregates will show phase-separated dynamics that are much more liquid-like and dynamic at the early stages, compared to the mature rigid structure. As a first step to understanding Buc regulation and aggregation we aimed to address the dynamics of Buc phase separation during Bb formation, following its initial polarization in symmetry breaking and towards its maturation. Evidence suggests Buc prion-like functions in zebrafish, but these have not been directly investigated.ourlab previously revealed that Buc is required specifically for nucleating Bb granules. In *buc*$^{-/-}$ oocytes, symmetry breaking and the initial Bb granule aggregation in the nuclear cleft we re normal (Elkouby et al., 2016). Only during Bb assembly, granules failed to nucleate and dispersed, preventing Bb formation (Elkouby et al., 2016). This concluded that Buc function is specifically required for granule nucleation at these stages, consistently with a prion-like function. Buc and its *Xenopus* ortholog XVelo are predicted intrinsically disordered proteins (IDP) (Bontems et al., 2009; Boke et al., 2016) that contain a predicted prion-like domain at their N-termini (Boke et al., 2016). Under certain conditions IDPs phase-separate and nucleate RNP granules (Banani et al., 2017). Moreover, prion and prion-like proteins have a propensity to fold into stacks of ß-sheets forming amyloid structures (Banani et al., 2017; Boke & Mitchison, 2016; Scialò et al., 2019). In *Xenopus*, the Bb is rigid, non-dynamic, resistant to harsh conditions, and forms fibrillar structures ex vivo (Boke et al., 2016). Furthermore, in vivo, the mature Bb stains positive with an amyloid-specific dye, Thioflavin T (ThT), that is indicative of its amyloid-like structure (Boke et al., 2016). ThT is a small molecule that fluoresces upon binding to amyloid fibrils and is an established amyloid specific dye (Xue et al., 2017). Indeed, XVelo has been proposed to be the structural glue that holds the organelles together and nucleates RNP granules in the *Xenopus* mature Bb structure (Boke et al., 2016; Boke & Mitchison, 2017). Therefore, we hypothesized that Buc may be the structural glue that holds the organelles together in the zebrafish Bb and is thus responsible for the amyloid-like properties within the mature structure.

Buc phase-separation in Balbiani body formation

Yet, the visualization and characterization of amyloid-like structures in the zebrafish Bb is severely lacking in the literature. Therefore, we beganourstudies of investigating the prion-like functions of Buc in zebrafish by testing for the formation of ß-sheets in the mature Bb structure using ThT. ThT

labeling detected presumptive amyloid ß-sheets specifically in the mature Bb in live ovaries (Fig. 7), that we re absent in ovaries not incubated with ThT as a control (Fig. 7B). These results are consistent with what was observed in the ThT labeling of mature Bb in *Xenopus* (Boke et al., 2016). To confirm ThT detection in the Bb we next performed live imaging of ThT together with Bb markers (Fig. 7A). To visualize Buc protein localization, we used a transgenic line expressing Buc-GFP [*Tg(buc:buc-gfp-buc 3'utr)*] (Riemer et al., 2015). This line contains the entire *buc* locus and was shown to be fully functional, as it rescues Bb formation, oocyte polarity, and fertility in *buc*$^{-/-}$ oocytes (Riemer et al., 2015). Therefore, Buc-GFP expressed from this transgene reliably reflects endogenous Buc protein dynamics, as shown in (Riemer et al., 2015). Live imaging of Buc-GFP, as we ll as of Bb-enriched mitochondria, using MitoTracker, confirmed the co-localization of ThT-positive presumptive amyloid ß-sheets in the Bb (Fig. 1A). Strikingly, ThT signals we re absent in *buc*$^{-/-}$ oocytes (Fig. 1A) providing the first genetic evidence for Buc dependent formation of presumptive amyloid fibrils in the Bb.

Biomolecular condensates have a range of physical properties and the potential to transition betwe en material states. The more solute-like condensates tend to be dynamic, disordered and have we ak interactions. The more solid-like condensates (i.e. amyloid fibers) are seemingly non-dynamic, rigid and have strong interactions. While the mature Bb is a more solid like structure showing amyloid ß-sheets, we wanted to determine the properties and dynamics of the Bb granules prior to their formation of the mature structure. we hypothesized that the early condensates may be more dynamic and have liquid-like phase separation properties prior to their maturation. The Buc-GFP line allows for the investigation of these biophysical properties in juvenile zebrafish ovaries, where oocytes of all relevant developmental stages can be observed live. Until now, investigating phase separation and the early formation of Bb granules in early oocytes has been almost impossible due to the technical challenges and a lack of protocols for live time-lapse analyses of whole juvenile ovaries. Howe ver, here we showe d that this barrier can be broken by utilizingourlab's methods for culturing and live imaging of juvenile Buc-GFP transgenic ovaries (Elkouby & Mullins, 2017b; Mytlis & Elkouby 2021).

To better address such dynamics, we performed live time-lapse imaging of cultured juvenile ovaries carrying the Buc-GFP transgenic line (Fig. 1B). we determined several types of Buc-GFP granule dynamics in vivo suggesting their early formation by phase separation and liquid droplet-like behavior. First, using laser scanning confocal microscopy (LSCM), we recorded granules that formed in real time, which gradually appear in a position where the Buc-GFP signal was not previously detected and appear to be condensing (Fig. 1B, pink arrows). In parallel, other parts of the main aggregate seemed

to dissolve over time (Fig. B, yellow arrows). These observations highlight the dynamic liquid-like nature of the Buc-GFP aggregate and are consistent with its condensation via phase separation in early oocytes.

Molecular condensates such as the Bb, and the IDR proteins that drive their phase separation like XVelo and Buc, are structurally dynamic and exhibit rapid internal molecular rearrangements and rapid exchange of molecules with the surrounding cytoplasm (Boke et al., 2016). Due to their dynamic and labile nature, liquid-like condensates are highly sensitive to shifts in temperature, pH, and other environmental factors (Dodson & Kennedy, 2020). we found that Buc-GFP was detected only in the pellet fraction of the oocyte extract and not in the soluble supernatant (Fig. 1C-E). In an attempt to shift Buc-GFP to the soluble supernatant fraction, we used L-Arginine (L-Arg), a reducing agent that increases solubility of large protein complexes. Indeed, we observed a shift in the detection of Buc-GFP protein from the insoluble pellet to the soluble supernatant fraction in a dose-dependent manner in the presence of 0.5-1.5M L-Arginine (Fig. 1E). These experiments confirmed that Buc-GFP forms insoluble molecular aggregates in oocyte extracts, and is lacking from the soluble fraction (Fig. 1E).

we hypothesized that Buc-GFP protein complexes in the insoluble pellet represent condensed large Bb complexes. we reasoned that if this is the case, then these complexes would be absent from similar pellet fractions of *buc*$^{-/-}$ oocytes. Therefore, we wanted to compare pellet fractions of *wt* versus *buc*$^{-/-}$ extracts by MS. we extracted protein from 20-100µm oocytes, from *wt* and *buc*$^{-/-}$ ovaries. In each genotype we performed size specific isolation of oocytes and isolated the supernatant and pellet fractions after centrifugation to send for MS (all samples we re run in triplicates). In *buc*$^{-/-}$ oocytes Bb granules are dispersed and fail to nucleate and assemble the Bb. Therefore, we expected Bb proteins to be detected as soluble proteins in the supernatant of *buc*$^{-/-}$ oocyte extracts and not be pelleted down since the Bb does not form in the mutant. These experiments allowe d for the identification of novel Bb proteins more broadly, some of which we re expected to be Buc binding candidates. During the subsequent analysis after MS, we therefore searched for proteins that we re enriched in the pellet over the supernatant fraction (P>S) in the *wt*, but not enriched in the pellet of *buc*$^{-/-}$ (Fig. 1F-G).

Gene Ontology (GO) enrichment analysis revealed that the proteins enriched in the *wt* pellet compared to the supernatant fraction highly associated with categories of biological processes including "RNA processing", "mRNA metabolic process" and "Ribonucleoprotein complex biogenesis" (Fig. 1G), as expected for Bb RNP complexes. In contrast, these we re not enriched in the pellet compared to supernatant fraction in the *buc*$^{-/-}$ extracts. In the *buc*$^{-/-}$ pellet compared to the supernatant fraction, the pellet was enriched in more general biological processes involving the cytoskeleton such as "Actin binding", "Motor Activity" and "Cytoskeleton Protein Binding" (Fig. 1G). The results from the

enrichment assay are particularly interesting since the Balbiani body forms specifically in early oocytes to compartmentalize RNP complexes (Elkouby et al., 2016). In mutants, when Buc is no longer present and the Bb fails to form, and the enrichment of these RNA processes GO terms is lost. Notable, these proteins we re not downregulated, but specifically shifted to the soluble supernatant fraction of *buc*$^{-/-}$ extracts, further indicating their dependency on Buc to form larger molecular complexes. These experiments provide biochemical evidence for the Buc-dependent formation of large insoluble RNA-protein complexes. Together with Buc-GFP live dynamics above conclude, these data conclude the phase separation mechanisms of Buc and condensation of the Bb.

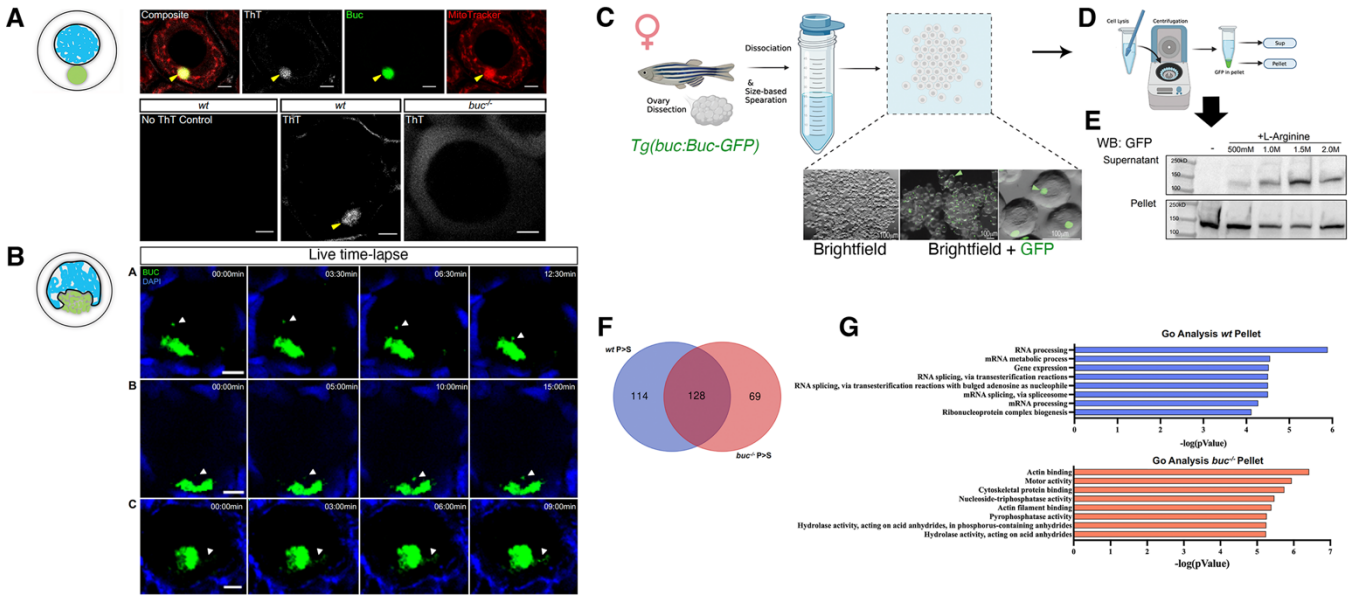

Figure 1. Buc phase-separates into prion-like condensate in the mature Bb. A. Top panels: Live imaging of Buc-GFP (green), ThT 20µM (grey) and MitoTracker (red), showing presumptive amyloid ß-sheets in the mature Bb (yellow arrowheads). n=6 ovaries. B**ottom panels:** ThT signals are absent in *buc*$^{-/-}$ oocytes. n=4 ovaries. Scale bar, 10μm in all images. **B.** Top: Dynamic behavior of a Buc-GFP granules showing movement in the X-Y axis (white arrow) that translocated to the main aggregate in the nuclear cleft. Middle: Buc-GFP granule that was not previously detected, but subsequently materialized over time and appeared to be condensing (white arrow). Bottom: Buc-GFP granule that condensed and immediately fused with larger granules in the main aggregate within the nuclear cleft. DAPI marked in blue. n=5 ovaries. Scale bar, 5μm. **C.** Stage specific isolation of oocytes from Buc-GFP ovaries, exhibiting GFP-positive Bb. **D.** A cartoon depicting the accumulation of Buc-GFP in the insoluble pellet of lysed and centrifuged oocytes. **E.** Detection of Buc-GFP in the pellet and not in the soluble supernatant, that is solubilized by a dose-dependent addition of L-Arg, shifting from the insoluble pellet fraction to the soluble supernatant fraction. **F.** Venn Diagram of pellet vs supernatant proteins, purple represents that proteins that were enriched in the *wt* pellet vs *wt* supernatant (P>S) and red represents proteins that were enriched in the *buc*$^{-/-}$ pellet vs *buc*$^{-/-}$ supernatant (P>S). **G.** GO analysis revealed that the proteins enriched in the *wt* pellet were highly associated with categories of biological

processes involving RNA processing while proteins enriched in the *buc*$^{-/-}$ pellet were associated with non-specific categories.

Early dynamics of Buc in Bb aggregation requires specialized organization of microtubules

Studies in *Xenopus* previously showe d that the mature Bb is a stable, resistant and rigid structure with very low rates of turnover with the cytoplasm (Boke et al., 2016). This stable nature of the Bb is further substantiated by the detection of amyloid fibrils in *Xenopus* (Boke et al., 2016), which we confirmed in zebrafish. This contrasts with Buc-GFP liquid droplet-like dynamics that we was able to record. To address this discrepancy, we aimed to determine Bb dynamics at different stages of its formation and test whether its dynamics during development differed from the mature compact structure. Thus, we performed fluorescence recovery after photobleaching (FRAP) analyses in live ovaries, measuring Buc-GFP turnover, as an indicator for Bb dynamics, in early stages of Bb formation, during nuclear cleft aggregation (oocytes at St. we diplotene, diameter of 22-40µm) and in the mature Bb (oocytes at St. we diplotene, diameter of 50-70µm) for comparison (Fig. 2).

we established adequate bleaching and imaging conditions for consistent bleaching betwe en individual aggregates within oocytes, betwe en different oocyte stages and across all experiments. we systematically bleached an area of approximately 1/3 of the aggregate size to around 20% of the original Buc-GFP intensity and then followe d recovery for 680 seconds (11.33min), recording every 2.5 seconds. These conditions we re established during initial calibration experiments. we observed that bleaching 1/3 of the aggregate resulted in a significant reduction in Buc-GFP signal without completely ablating all the protein in the nuclear cleft. Moreover, we observed a plateau of recovery dynamics after 680 seconds. Therefore, to reduce any photobleaching affects, all experiments had a duration of 680 seconds. Subsequently, we plotted recovery curves and calculated the immobile/mobile fractions in order to determine Buc protein dynamics and turnover in individual oocytes. The immobile fraction is the incomplete recovery observed at the site of bleaching (beach spot) due to some fraction of the molecules that are immobilized. The mobile fraction is the rest of the molecules that contribute to the fluorescence recovery. Calculating the immobile/mobile fractions has been deemed the most representative and comprehensive way for analyzing FRAP data (Blumenthal et al., 2015; Giakoumakis et al., 2017; Houtsmuller 2005; Kang et al., 2015). Initially, we recorded 10 pre-bleach frames and after background subtraction, the average intensity was used as pre-bleach intensity. Post-bleach frames we re background

subtracted and to make replicates comparable, post-bleach frame #1 of each measurement was set to 0 and corresponding pre-bleach intensity was corrected for this (see Methods).

First, we found that the mature Bb revealed very little recovery and 11 minutes after the initial photobleaching occurred, the bleached area (Fig. 2B, red box) contained almost no Buc-GFP signal (Fig. 2B & C). Additionally, the mobile fraction which represents the recovered molecules reached only 13% compared to the immobile fraction which reached a high of 87% (Fig. 10D). This shows that the zebrafish Bb is similar to and consistent with the stable structure of the *Xenopus* Bb previously reported (Boke et al., 2016). In contrast, at nuclear cleft stages (oocytes at St. we diplotene, diameter of 22-40µm), Buc-GFP showe d a much more significant recovery at around 40-50% of the initial intensity, within the allotted recovery time (Fig. 2A & C). Buc-GFP turnover was higher, showing a faster recovery, where the bleached area (Fig. 2A, red box) gained significant signal as early as 3 minutes after photobleaching. Moreover, the mobile fractions increased to 56% versus only 13% in the mature structure (Fig. 2D). Thus, both the extent and rate of recovery confirm that Buc-GFP turnover is significantly faster at early aggregation stages and ultimately ceases in the mature compact structure where the majority of the protein is immobile. This can be further observed on an individual oocyte basis in the plots of the immobile (Fig. 2E) and mobile fractions (Fig. 2F). Lastly, to take a closer look at these dynamics, we plotted the last 20 frames of FRAP experiments (Fig. 2G), where the average curves differed most significantly (Fig. 2C). These results show a sizeable difference in the relative fluorescent intensity, highlighting the immobility of the Buc protein in the mature structure (Fig. 2G). Additionally, as a control for cell viability and to rule out any potential cell damage artifacts, we incubated ovaries with MitoTracker, which selectively labels live and active mitochondria, confirming their normal viability after FRAP (Fig. 2H). we confirmed that the MitoTracker signal was unchanged from the pre-FRAP oocyte compared to the post-FRAP oocyte (Fig. 2H), validating mitochondria activity and cell viability and thus ruling out cell damage artifacts. Taken together, these results argue that Bb formation follows a gradual condensation process, where smaller phase-separated granules are much more dynamic and continue to form and/ or seed new Buc proteins, while the aggregate continues condensing until it becomes very stable, presumably when all IDR interactions are saturated and amyloid ß-sheets form.

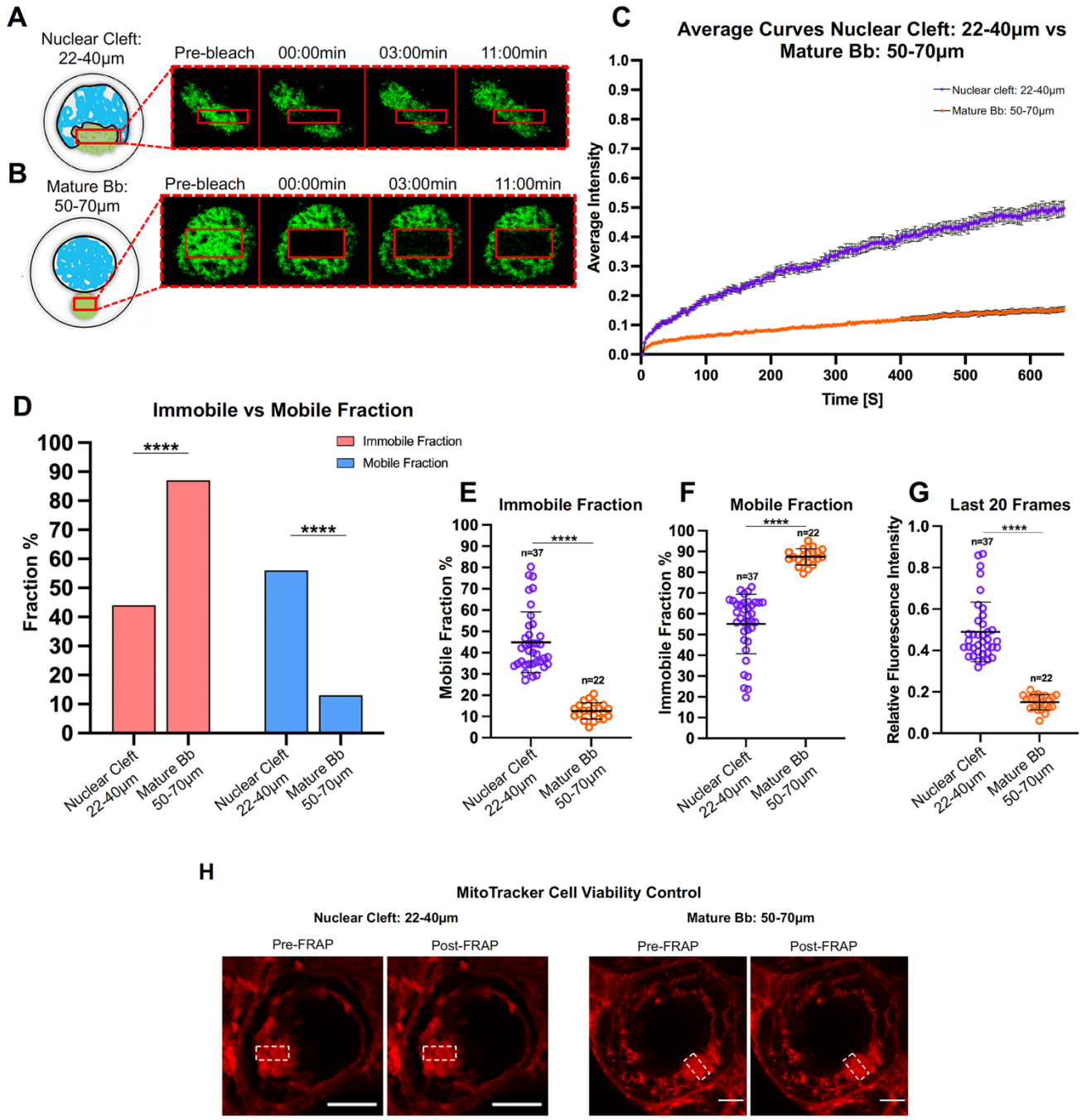

Figure 2. FRAP Dynamics in the Mature Bb Structure vs Early Stages of Bb Formation. **A**. Montage of an early oocyte in nuclear cleft stage (22-40µm) during FRAP. Buc-GFP signal recovers significantly starting as early as 3 minutes (red box). **B**. Montage of an oocyte containing mature Bb (50-70µm). Little to no recovery is observed even after 11 minutes (red box). **C**. Average curves of early stages of Bb formation during nuclear cleft stages (oocytes at St. I diplotene, diameter of 22-40µm n=37 oocytes from 8 ovaries) and in the mature Bb (oocytes at St. I-mid-diplotene, diameter of 50-70µm; n=22 oocytes from 6 ovaries). Buc-GFP turn over in early oocytes (22-40µm) is much

greater. Plot shows average intensity with SEM. **D**. Immobile vs Mobile Fractions for both oocyte size groups. Earlier oocytes are more dynamic and have a great mobile fraction than the oocytes with mature Bbs. **E-F**. Separate plots for mobile and immobile fractions showing the mean and SD for each group. **G**. Plots of the last 20 frames of FRAP experiments where the average intensities for each group were the most significantly different. Plots show the mean and SD for each group. **H**. Cell viability assay using MitoTracker showing that mitochondria retain signal after FRAP. ROI of bleached area (white box). n=3 ovaries. Scale bar, 10µm in all images.

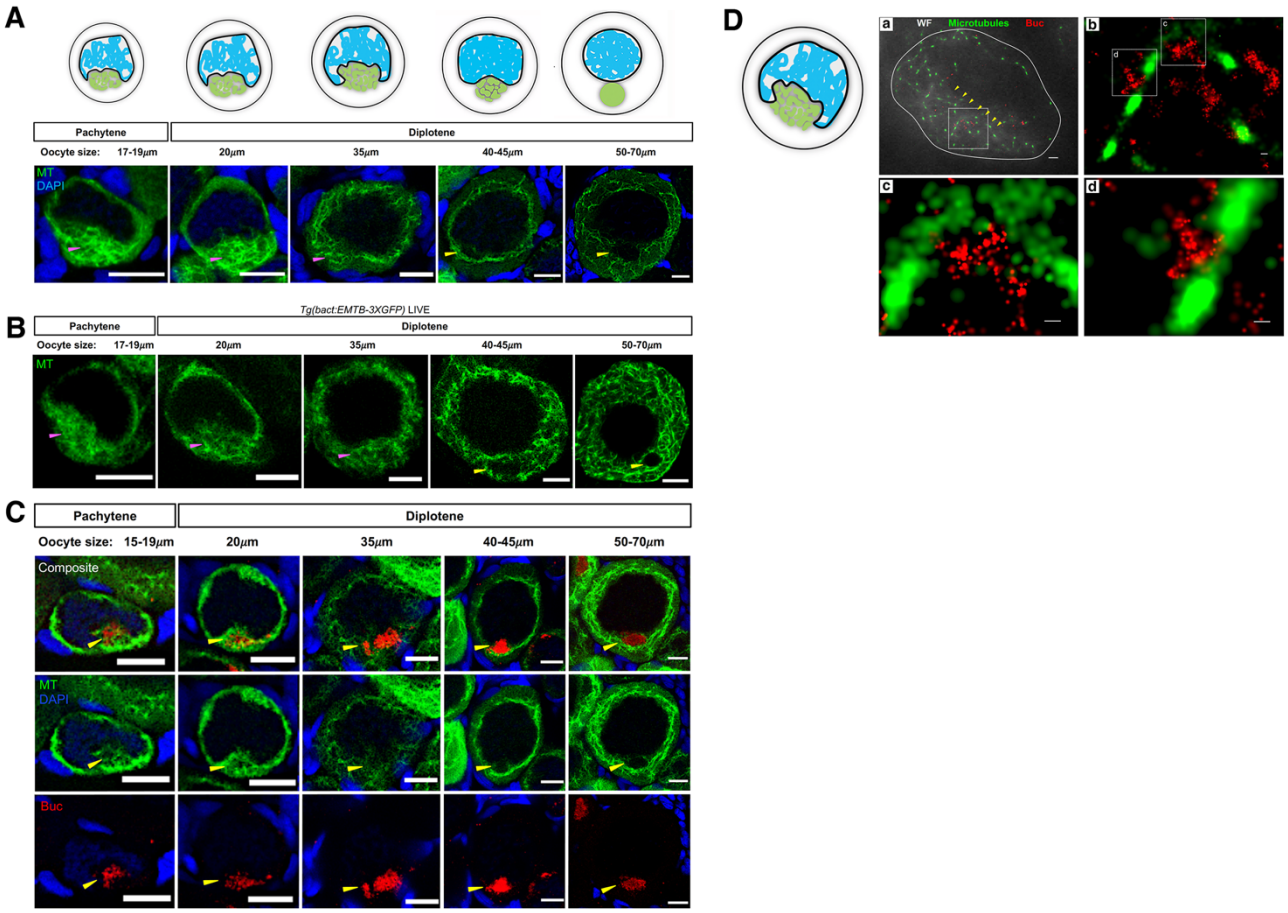

Figure 3. Buc aggregates are adjacent to microtubule cables that are organized in a transient meshwork in the nuclear cleft. A. Fixed (A) and live (B) images of *Tg(bact:EMTB-3XGFP)* ovaries, exhibiting elaborated meshwork of MTs cables specially within the nuclear cleft of oocytes (pink arrows) starting from pachytene diameter of 17-19µm up until St. I diplotene, diameter of 22-40µm. Elaborated meshwork of MTs cables was specifically excluded from the presumptive Bb region forming a cage-like organization around it (yellow arrows). Scale bar, 5*µ*m in left two images and 10*µ*m in right three images for both panels. n=3 ovaries in A, and n=8 ovaries B. **C.** Co-labeled *Tg(bact:EMTB-3XGFP)* (green) ovaries with Buc antibody (red). In early oocytes (17-40µm) elaborated meshwork of MTs cables within the cleft intertwined with Buc granules. At later stages (50-70µm) MT were excluded

from the maturing Bb and formed a cage-like structure around it. Yellow arrows mark the nuclear cleft region. n=6 ovaries. Scale bar, 5μm in left two images and 10μm in right three images. **D.** Super-resolution (dSTORM) images of oocytes from co-labeled *Tg(bact:EMTB-3XGFP)* ovaries with Buc antibody (red). a) Wide field (WF) image reveals early oocyte structure and nuclear cleft (yellow arrows). Scale bar, 1μm. b) Close up of MT and Buc protein aggregates in the nuclear cleft. Scale bar, 0.1μm. c) Buc in close proximity to MT cables. Scale bar, 0.1μm. d) Buc MT interface. Scale bar, 0.1μm.

Interactions between IDRs that induce the formation of RNP granules require a local concentration of the IDR protein above a threshold. However, the regulation of the recruitment of IDR proteins over their required threshold, their IDR interactions, as we ll as the regulatory proteins that control their rate and extent of condensation are largely unknown, especially in vertebrates. An active localization mechanism could localize Buc to the nuclear cleft, increasing its local concentration and allowing it to condense into small granules that can then aggregate to form a mature, more solid phase-separated structure.ourlab previously determined that microtubules (MTs) were required for the earlier localization of Bb granules during the preceding symmetry breaking stages (Elkouby et al., 2016).ourwork now uncovers the continuous supply of Buc to the aggregating Bb at cleft stages beyond these events. Therefore, microtubules are a promising candidate for localizing Buc during phase separation in the cleft as we ll.

As a first step to specifically address the role of MTs in Buc dynamics and Bb formation we wanted to visualize the organization of MT in oocytes and characterize their developmental organization during the early stages of Bb formation. By using a transgenic microtubule reporter line, [*Tg(bact:EMTB-3XGFP*] (Revenu et al., 2014), in both fixed ovary samples using immunostaining (Fig. 11, top panel) and by live imaging of transgenic ovaries (Fig. 3A-B), we detected an elaborated meshwork of MTs cables specially within the nuclear cleft of oocytes (Fig. 3A-B, pink arrows) starting from pachytene stages (diameter of 17-19µm) up until St. we diplotene (diameter of 22-40µm). In contrast, in mature Bb stages (St. we diplotene, diameter of 50-70µm), instead of the elaborated network of MT cables that we detected in earlier stages, MT cables we re interestingly specifically excluded from the presumptive Bb region, forming a cage-like organization around it (Fig. 3A-B, yellow arrows).

To definitively determine how this developmentally dynamic microtubule organization correlates with Bb formation, we co-labeled *Tg(bact:EMTB-3XGFP)* ovaries with Buc antibody (Fig. 3C). This confirmed that **(1)** in early oocytes (17-40µm) MT organized in a meshwork within the cleft that intertwined with Buc granules (Fig. 11 & 12), and **(2)** at later stages (50-70µm) MT w re excluded from

the maturing Bb and formed a cage-like structure around it (Fig. 3A-C). This dynamic developmental organization of MT that is concomitant with Bb formation, confirm that MTs are present at the right developmental time and within the correct cellular location to play a role in Buc condensation.

To further confirm the potential spatial interactions of MT cables and Buc, we performed super-resolution microscopy (by stochastic optical reconstruction microscopy – dSTORM) on whole EMTB-GFP ovaries co-labeled for GFP (MT) and Buc (Fig. 3D). The spatial resolution in ovaries achieved by this technique was ~20nm. Interestingly, we observed Buc granules in close proximity to MTs (Fig. 3D) and even points where they interfaced (Fig. 3D) along the cables in oocytes, both within the nuclear cleft and in non-cleft cytoplasm. Altogether, these results suggest that MT localize Buc during its phase separation and Bb granule condensation, likely by active trafficking.

Next, to functionally test the roles of MT in Buc dynamics and Bb formation we performed FRAP experiments on Buc-GFP ovaries that we re treated by two different established MT depolymerizing drugs, nocodazole and colchicine (Fig. 4). First, we determined that MTs are depolymerized after incubation of cultured ovaries in 20µM nocodazole for 90min and by 50µM colchicine for 90min, in identical settings to our FRAP experiments by live imaging of EMTB-GFP ovaries (Fig. 4A). Next, we performed FRAP experiments after treatment with each drug or a DMSO control, analyzing Buc-GFP recovery at the early stages of Bb formation during nuclear cleft aggregation (oocytes at St. we diplotene, diameter of 22-40µm) (Fig. 4B & C).

we found that depolymerization by either nocodazole or colchicine completely abolished Buc-GFP recovery, in contrast with control treatments by DMSO (Fig. 4D & F). While the DMSO control group revealed an average mobile fraction of 41%, similar to what was observed with the normal, non- treated culture conditions, the nocodazole treated group dropped to 15% mobile fraction (Fig. 4D, E & H). Likewise, the colchicine treated group revealed a drop in the average mobile fraction to 10% from 36% in the DMSO control group (Fig. 4F, G & I). This can be further observed on an individual oocyte basis in the plots of the immobile and mobile fractions for both nocodazole and colchicine treated groups. To take a closer look at these dynamics, we plotted the last 20 frames of FRAP experiments, where the average curves differed most significantly. These results show a large difference in the relative fluorescent intensity, highlighting the immobility of the Buc protein when MT are depolymerized. Lastly, as a viability control, we incubated ovaries with MitoTracker, confirming their normal viability after drug treatment (Fig. 4J & K). we confirmed that the MitoTracker signal was unchanged after both

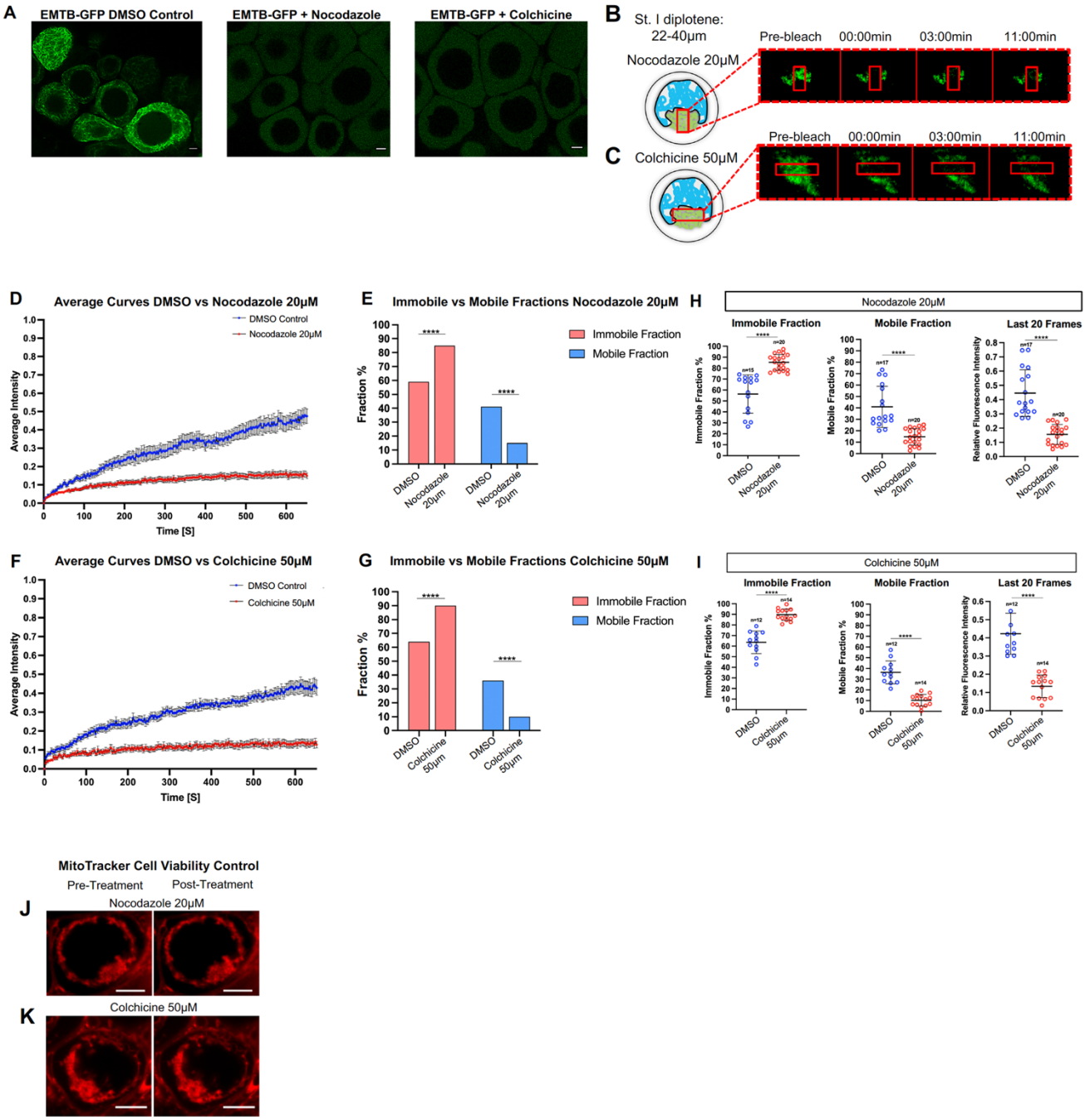

Figure 4. Buc turn-over in the cleft requires microtubules. A. MTs are depolymerized after incubation of cultured ovaries in 20µM nocodazole for 90min (n=3 ovaries) and by 50µM colchicine for 90min (n=3 ovaries). Scale bar, 10µm. **B**. Montage of an early oocyte (22-40µm) treated with 20µM nocodazole during FRAP. Buc-GFP signal has little to no recovery even after 11 minutes (red box). **C**. Montage of an early oocyte (22-40µm) treated with 50µM colchicine during FRAP. Similar to nocodazole treatment, little to no recovery is observed (red box). **D**. Average curves of early stages of Bb formation during nuclear cleft stages (oocytes at St. I diplotene, diameter of 22-40µm) treated with DMSO control (n=17 oocytes from 4 ovaries) or 20µM nocodazole (n=20 oocytes from 5 ovaries). Plot shows average intensity with SEM. **E**. Average Immobile vs Mobile fractions for both DMSO control or 20µM nocodazole groups. **F**. Average curves of early stages of Bb formation during nuclear cleft

stages (oocytes at St. I diplotene, diameter of 22-40µm) treated with DMSO control (n=12 oocytes from 3 ovaries) or 50µM colchicine (n=14 oocytes from 3 ovaries). Plot shows average intensity with SEM. **G**. Average Immobile vs Mobile fractions for both DMSO control or 50µM colchicine. **H**. Individual plots of immobile, mobile and the last 20 frames of oocytes treated with DMSO control or 20µM nocodazole. Plots show the mean and SD for each group. **I**. Individual plots of immobile, mobile and the last 20 frames of oocytes treated with DMSO control or 50µM colchicine. Plots show the mean and SD for each group. **J**. Cell viability assay using MitoTracker, mitochondria retain signal after treatment with 20µM nocodazole (n=4 ovaries). **K**. Similarly, mitochondria retain signal after treatment with 50µM colchicine (n=3 ovaries).

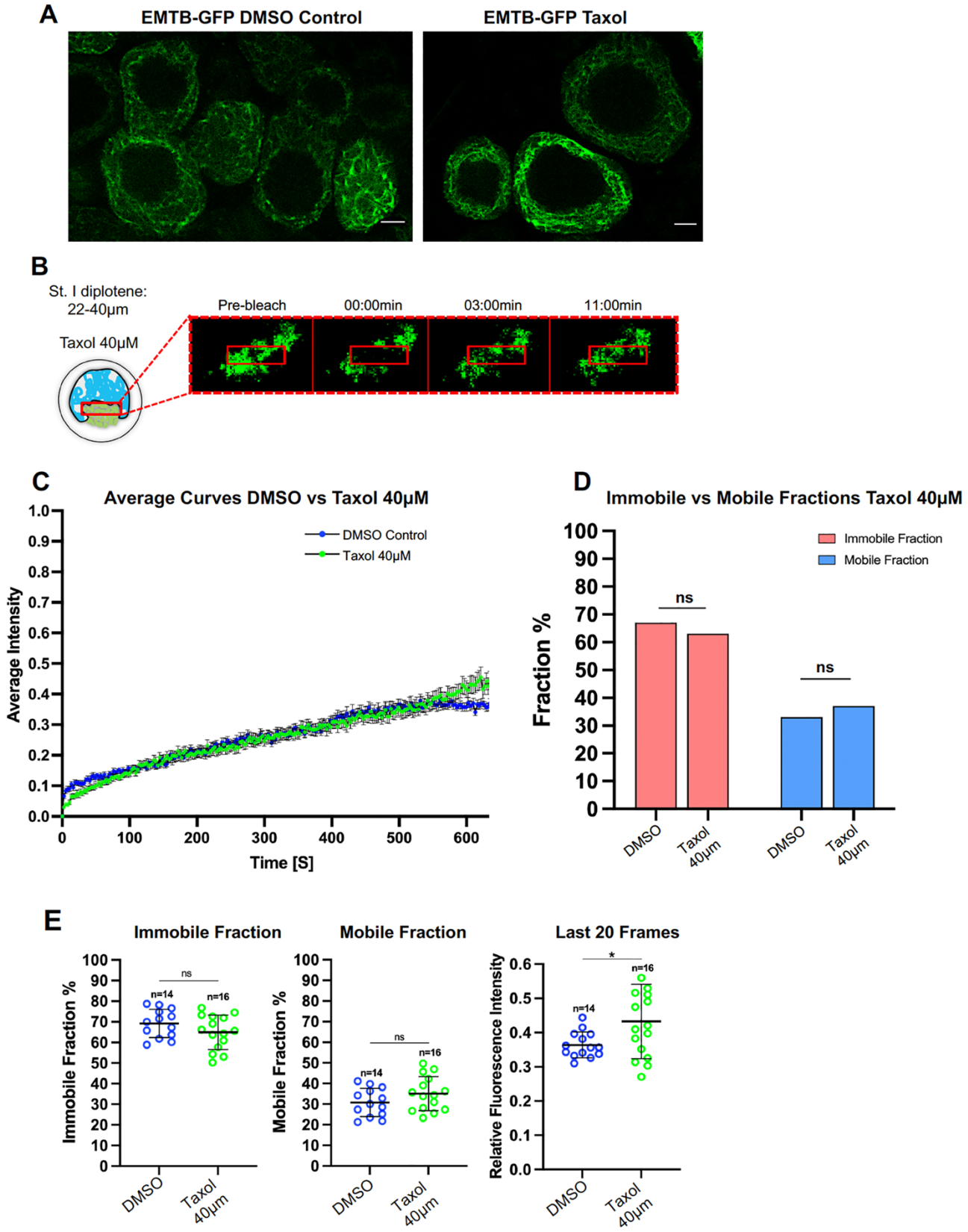

Figure 5. Normal Buc turn-over upon microtubule stabilization by Taxol. **A**. Oocytes from ovaries treated with 40µM of taxol for 90min showed normal MT organization (n=3 ovaries) when compared to DMSO control (n=2 ovaries). Scale bar, 10µm. **B**. Montage of an early oocyte (22-40µm)

treated with 40µM taxol during FRAP. Recovery indistinguishable from DMSO control or normal culture conditions. **C**. Average curves of early stages of Bb formation during nuclear cleft stages (oocytes at St. I diplotene, diameter of 22-40µm) treated with DMSO control (n=14 oocytes from 3 ovaries) or 40µM taxol (n= 16 oocytes from 3 ovaries). Plot shows average intensity with SEM. **D**. Immobile vs Mobile fractions for both DMSO control or 40µM taxol. **E**. Individual plots of immobile, mobile and the last 20 frames of oocytes treated with DMSO control vs taxol. Plots show the mean and SD for each group.

drug treatments, validating mitochondria activity and cell viability, and ruling out toxicity artifacts (Fig. 4J & K).

As an additional control for the specificity of the nocodazole and colchicine effects, we treated ovaries with another MT manipulating small molecule, the MT stabilizing drug taxol. Oocytes from ovaries treated with 40µM of taxol for 90min showe d normal MT organization (Fig. 5A), as we ll as Buc-GFP recovery that was indistinguishable from DMSO control or normal culture conditions (Fig. 5B, C & D). Likewise, plots of individual oocytes showing the immobile and mobile fractions of taxol compared to DMSO further highlight the similarity betwe en the two groups (Fig. 5E). Howe ver, when we plotted the last 20 frames of FRAP experiments, where the average curves differed most significantly (Fig. 15C), there was a slight statistical difference betwe en the taxol and DMSO treated groups (Fig. 15E, rightmost plot). From this data, we was able to conclude that MTs are required for Buc-GFP turnover within the Bb condensate during its formation.

Buc Granules are Trafficked on Microtubules by Dynein

MT could localize Buc granules via either trafficking by a motor protein, or by exerting dynamics that mechanically elicit movement of Buc in the cytoplasm. MT dynamics for movement require their constant depolymerization and polymerization. Treatments by inhibiting MT depolymerization by taxol, likely resulted in the generation of more stationary cables.ourfindings that taxol did not inhibit Buc-GFP recovery, suggest that their dynamics are not likely a major contribution to its localization. Additionally, since it was previously established that Buc localizes around the centrosome during symmetry breaking and cleft aggregation stages (Elkouby et al., 2016), its potential trafficking would likely require the minus (-) end motor protein dynein. To test whether dynein was required for Buc-GFP recovery, we used the dynein inhibitor ciliobrevin in conditions where we previously determined that other meiotic dynein functions in the oocyte are inhibited (25µM, 90min) (Mytlis, Kumar et al., 2021, biorxiv). we performed Buc-GFP FRAP experiments in ovaries treated with 25µM ciliobrevin for 90min, and found that dynein inhibition completely abolished Buc-GFP recovery similar to what was observed when MT we re

depolymerized (Fig. 6). Ciliobrevin treatment had a potent effect on the average mobile fraction which reached just 7% compared to 35% in the DMSO control group (Fig. 6C, D & E). These results combined with the individual oocyte plots for the immobile, mobile and last 20 frames (Fig. 6F) show that dynein function is required for Buc-GFP recovery. Again, to rule out cell death as a possible reason for lack of Buc-GFP recovery, we used MitoTracker as a cell viability control (Fig. 6F) consistent with all prior FRAP experiments. Indeed, we confirmed that the MitoTracker signal was unchanged after drug treatment and thus cells we re normally viable.

Dynein serves multiple roles in cells, and in certain contexts can anchor MTs to control their organization (Burakov et al., 2008; Delanoue & Davis, 2005). Therefore, dynein may be required for Buc localization directly by a trafficking mechanism or indirectly by affecting MT organization. To distinguish betwe en these models, we analyzed MT organization by live imaging in ciliobrevin treated EMTB-GFP ovaries (Fig. 6A). MT organization was consistent with their organization in non-treated and DMSO ovaries, normally exhibiting the MT meshwork within the cleft and generally in the oocyte (Fig. 6A).

These results demonstrate the MT organization is not disrupted by dynein inhibition and the diminished recovery rates observed with ciliobrevin are not likely due to mis-organized MTs. To confirm this, we treated ovaries with either DMSO control, or 40µM taxol (alone), or with both 40µM taxol + 25µM ciliobrevin. In these conditions, taxol would stabilize MTs prior to the treatment with ciliobrevin, assuring their intact appropriate organization upon dynein inhibition, which should still allow trafficking. Indeed, we confirmed that MT organization in taxol + ciliobrevin treated ovaries is similar to taxol alone and to DMSO control treated ovaries, showing that MT organization is normally intact under these conditions (Fig. 7A). In this case, if dynein is required specifically for Buc trafficking, even though the MT cables are present, the loss of dynein trafficking activity will inhibit Buc-GFP recovery. Consequently, if Buc-GFP recovery will be decreased by ciliobrevin treatment, it would most likely not be due to MT mis-organization by dynein loss of function, but rather due to loss of trafficking. we then preformed FRAP on Buc-GFP in these experimental groups described above. Indeed, oocytes in taxol (alone) treated ovaries showe d Buc-GFP recovery that was similar to DMSO control treated ovaries (Fig. 7B), consistent withourprevious results using taxol. Howe ver, in ovaries treated by a combination of taxol + ciliobrevin, recovery was abolished similar to ciliobrevin treatment alone with a decrease in mobile fraction to 15% compared to 36% in the taxol control group (Fig. 7C & D). These results combined with the individual oocyte plots for the immobile, mobile and last 20 frames (Fig. 7E) show that dynein function is required for Buc-GFP recovery even when MTs are stabilized. Again, to rule out

cell death as a possible reason for lack of Buc-GFP recovery, we used MitoTracker as a cell viability control (Fig. 7F) consistent with all prior FRAP experiments. we confirmed that the MitoTracker signal was unchanged after drug treatments and thus cells we re normally viable. While we cannot completely rule out other dynein functions, these results suggest that dynein is required mostly for directly trafficking Buc-GFP on MTs. Thus, we conclude that Buc localization by dynein trafficking on MT is required for its turnover in the forming Bb condensate, and for its continuous supply during granule nucleation and Bb formation.

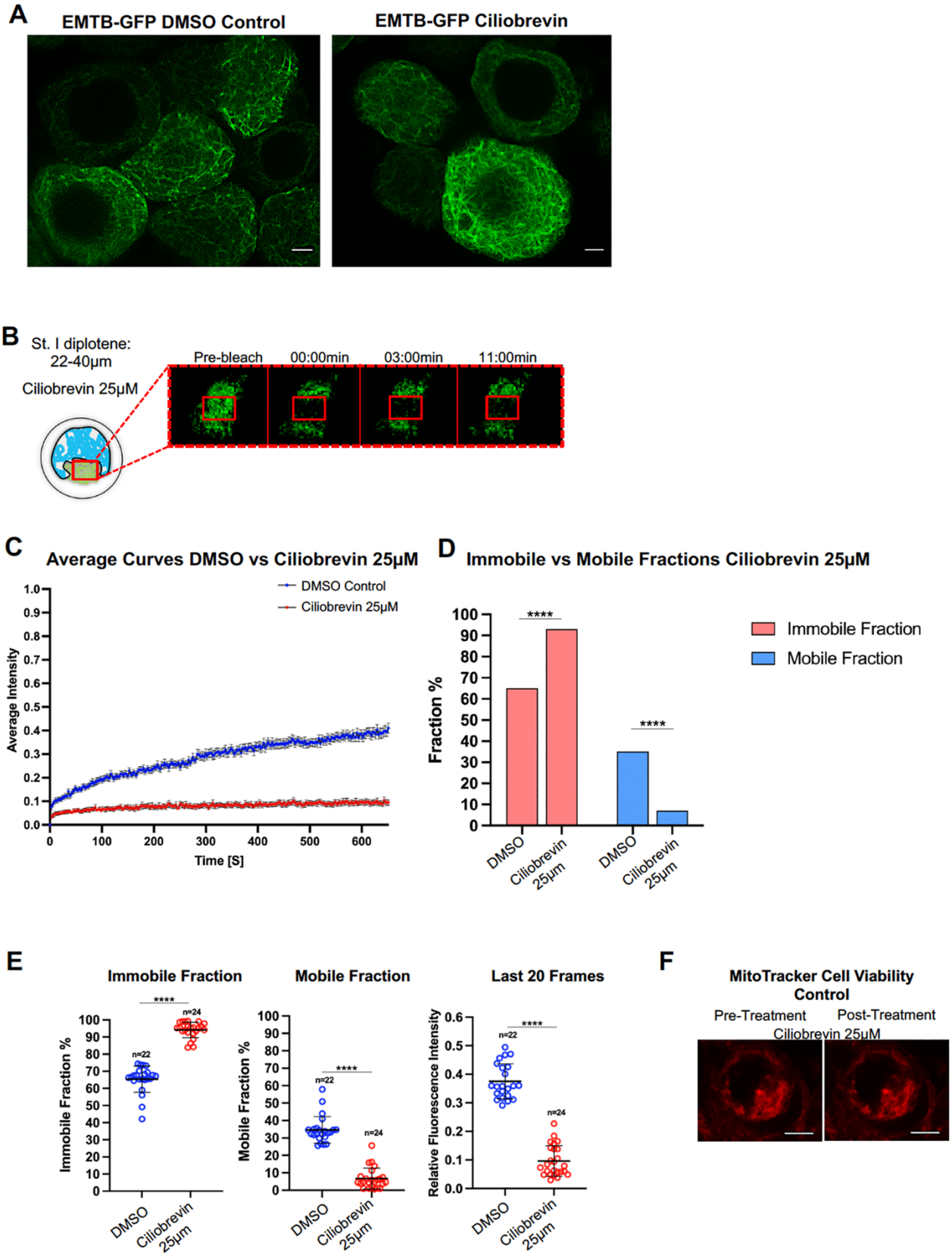

Figure 6. Buc turn-over requires Dynein activity. **A**. Oocytes from ovaries treated with 25µM of ciliobrevin for 90min showed normal MT organization (n=3 ovaries) when compared to DMSO control (n=2 ovaries). MT organization is not disrupted by dynein inhibition. Scale bar, 10µm. **B**.

Montage of an early oocyte (22-40µm) treated with 25µM ciliobrevin during FRAP. Dynein inhibition completely abolished Buc-GFP recovery similar to what was observed when MT were depolymerized. **C**. Average curves of early stages of Bb formation during nuclear cleft stages (oocytes at St. I diplotene, diameter of 22-40µm) treated with DMSO control (n=22 oocytes from 5 ovaries) or 25µM ciliobrevin (n=24 oocytes from 5 ovaries). Plot shows average intensity with SEM. **D**. Immobile vs Mobile fractions for both DMSO control or 25µM ciliobrevin. Ciliobrevin treatment had the most potent effect on the average mobile fraction. **E**. Individual plots of immobile, mobile and the last 20 frames of oocytes treated with DMSO control vs 25µM ciliobrevin. Plots show the mean and SD for each group. **F**. Cell viability assay using MitoTracker, cells retain signal after treatment with 20µM ciliobrevin (n=3 ovaries). Scale bar, 10µm.

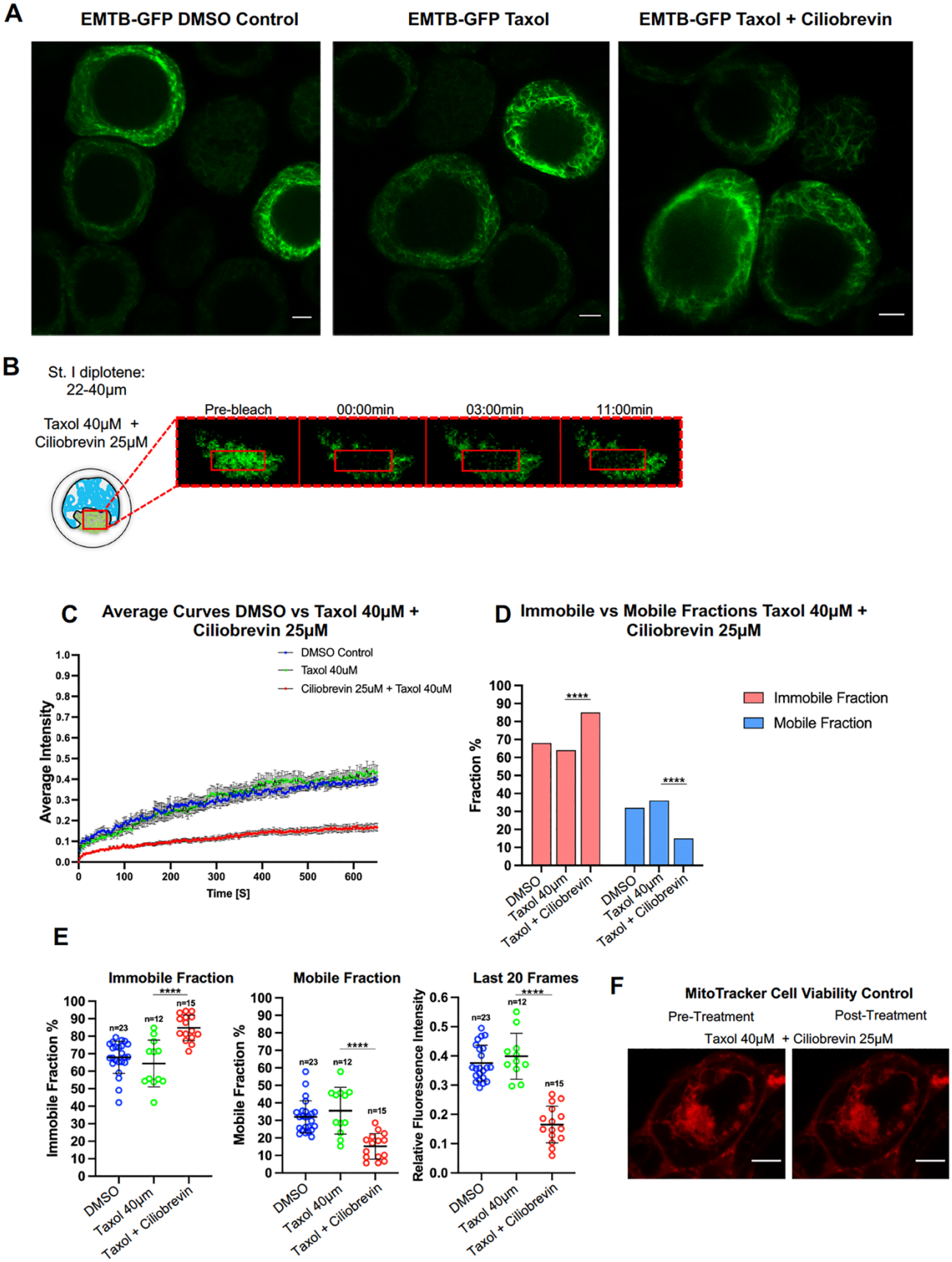

Figure 7. Dynein-mediated trafficking on microtubules is required for Buc turn-over. A. Oocytes from ovaries treated with 40 µM of taxol + ciliobrevin 25µM for 90min showed normal MT

organization (n=2 ovaries) when compared to DMSO (n=2 ovaries) and taxol (n=2 ovaries) controls. MT organization is not disrupted by dynein inhibition with the combination of taxol. Scale bar, 10µm. **B**. Montage of an early oocyte (22-40µm) treated with both 40 µM of taxol + ciliobrevin 25µM during FRAP. Dynein inhibition abolished Buc-GFP recovery even with the addition of MT stabilizing drug taxol. **C**. Average curves of early stages of Bb formation during nuclear cleft stages (oocytes at St. I diplotene, diameter of 22-40µm) treated with DMSO control (n=23 oocytes from 4 ovaries), 40 µM of taxol alone (n=12 oocytes 3 ovaries) or 40 µM of taxol + ciliobrevin 25µM (n=15 oocytes from 3 ovaries). Plot shows average intensity with SEM. Oocytes in taxol treated ovaries showed Buc-GFP recovery that were similar to control DMSO treated ovaries. However, in ovaries treated by a combination of taxol and ciliobrevin, recovery was abolished similar to ciliobrevin treatment alone. **D**. Immobile vs Mobile fractions for DMSO control, 40 µM taxol control or 40 µM taxol + 25µM ciliobrevin. **E**. Individual plots of immobile, mobile and the last 20 frames of oocytes treated with DMSO, 40 µM taxol controls or 40 µM taxol + 25µM ciliobrevin. Plots show the mean and SD for each group. **F**. Cell viability assay using MitoTracker, cells retain signal after treatment with both 40 µM taxol + 25µM ciliobrevin (n=3 ovaries). Scale bar, 10µm.

Discussion

The question of how membraneless compartments form is under intense investigation and gaining attraction in cell and developmental biology. In addition to driving germ granule formation, phase separation-related processes likely coordinate other aspects of germline development. The Balbiani body is great interface for studying the compartmentalization of protein, RNA, and various membrane-bound organelles into a large, membraneless compartment in vertebrate oocytes. In *Xenopus*, the Bb is rigid, seemingly non-dynamic, resistant to harsh conditions ex vivo, and stains with an amyloid-specific dye (Boke et al., 2016). Howe ver, unlike amyloids in pathological prion-like aggregates, amyloid formation in the Bb is reversible, and the Bb disassembles at later stages of oocyte development to establish its polarity axis (Elkouby 2017; Jamieson-Lucy & Mullins, 2019; Kloc et al., 2004). To account for all these properties of the Bb, we hypothesized that the Bb initially assembles via liquid phase separation, but then condenses into a solid-like state by forming an amyloid-like matrix (Dodson & Kennedy, 2020; Elkouby et al., 2016; Woodruff et al., 2018). While there is a lot of data exploring the properties of the mature Bb, very little is known about the early dynamics and initiation of the phase separation process that occurs in early oocyte development.

Here, by analyzing Buc dynamics in early Bb formation, by confocal, live imaging, FRAP and super-resolution microscopy, we was able to demonstrate Buc phase separation for the first time, and unravel the mechanisms of its Bb assembly. First,ourdata allows for the visualization of Buc liquid

droplet-like behavior in vivo, where smaller Buc granules join together over time to form a final Bb aggregate within the nuclear cleft of oocytes. Secondly, FRAP experiments reveal the initial dynamic nature of the early Buc protein aggregates in vivo compared to the seemingly static non-dynamic nature of the mature Bb aggregate. Thirdly, we was able to demonstrate that MT organize specifically in the cleft during Bb formation, interface with localizing Buc granules, and are required for their turnover via dynein trafficking. Finally, we provide evidence showing that Buc functions in zebrafish are required for the formation of amyloid ß-sheets in the mature, fully condensed Bb, likely through its prion-like domain.

Microtubules are Required to Localize Buc for Phase Separation Compatible Concentrations

How local concentrations of molecular condensates are controlled to trigger or prevent phase separation is poorly understood. Here, we functionally test the role of microtubules in Buc dynamics and Bb formation during early oocyte development. While previous studies in *Xenopus* and zebrafish showe d that MT depolymerization does not affect the mature compact Bb structure (Boke et al., 2016; Escobar-Aguirre et al., 2017b) the literature investigating the potential role of MTs in early oocyte development and the dynamics prior to Bb formation is severely lacking and unclear. Here, we show that localization and polarization of Bb granules at stages proceeding symmetry breaking require MTs and specifically the minus (-) end motor dynein. In mature Bb stages, there is an elaborated network of MT cables in the oocyte that is interestingly specifically excluded from the Bb. In contrast, we show that during early and mid-cleft aggregation stages, there is an elaborated meshwork of MT cables specifically within the cleft that are intertwined with Buc. Additionally, for the first time in zebrafish,ourdata shows the cutting-edge spatial resolution of nearby Buc granules and MTs in the early cleft using super-resolution microscopy.

The results discussed above show that Buc granules are being actively trafficked from the cytoplasm to the nuclear cleft during oocyte differentiation and greatly contrast the mature structure. It is interesting to speculate that the MT network surrounding the mature Bb could have a structural role that limits Bb size and movement in the mature oocyte. The cage-like organization of the MTs at later stages could help control the size of the large aggregate by stopping the coalescence or fusion process of granules over time (Hyman et al., 2004). In this case the MT cage-like network could prevent coarsening (and subsequent Bb growth) by providing a physical barrier. Thus, holding the mature Bb in place prior to its translocation to the oocyte cortex, where it will eventually dissociate and unload its RNPs to specify the vegetal pole of the oocyte. Future studies are required to test this hypothesis.

While very little is known about the molecular mechanisms that govern Bb formation and disassembly, forward maternal-effect genetic screens in zebrafish identified two genes that regulate some of these processes, *bucky ball* (*buc*) (Dosch et al., 2004) and *microtubule actin cross-linking factor 1* (*macf1*) (Bontems et al., 2011; Gupta et al., 2010). As previously discussed, Buc is the only known protein required for Bb formation and without it, the Bb fails to form resulting in radially symmetric eggs (Bontems et al., 2009; Elkouby 2017; Heim et al., 2014; Marlow & Mullins, 2008; Riemer et al., 2015). Macf1 is required at later stages of oocyte differentiation when the Bb needs to localize to the oocyte cortex and disassemble (Escobar-Aguirre et al., 2017a; Elkouby, 2017; Gupta et al., 2010). Contrary to what is observed in the *buc-/-* mutant oocytes, the Bb in the *macf1*$^{-/-}$ mutants does form (Bontems et al., 2011; Dosch et al., 2004; Gupta et al., 2010). Howe ver, it fails to localize to the oocyte plasma membrane and disassemble, thus trapping the vegetally-fated mRNAs within the cytoplasm and preventing their final localization (Elkouby, 2017; Escobar-Aguirre et al., 2017a; Gupta et al., 2010). *macf1*$^{-/-}$ mutants have a phenotype of an enlarged Bb that is no longer in the correct position within the oocyte (Gupta et al., 2010). It is likely that the Bb interacts with various cytoskeletal elements when unloading its RNP granules on the cortex and it was shown that Macf1 mediates microtubule and actin connections to achieve proper disassembly (Elkouby, 2017; Escobar-Aguirre et al., 2017a; Gupta et al., 2010).

Howe ver, the potential role of MTs and their involvement in the localization of phase-separated aggregates in vivo is almost completely unexplored.ourlab previously determined that MTs we re required for earlier localization of Bb granules during the preceding symmetry breaking stages of oocyte development (Elkouby et al., 2016).ourwork here uncovers the continuous supply of Buc to the aggregating Bb at cleft stages beyond these events. In the literature, molecular condensation is often viewe d as a self-assembly process. Here, we propose a novel paradigm for the cellular control over condensation mechanisms by microtubules and specific dynein dependency in early oocyte development. Thus, concluding that microtubules organize multiple steps in Bb condensation and play an active role in trafficking early aggregates to the nuclear cleft allowing for nucleation and maturation of the mature Bb structure.

Self-Assembly of Phase-Separated Granules and Cellular Control

Molecular condensation is often viewe d as a self-assembly process where molecules will phase-separate once they reach their solubility limit or threshold concentration in solution (Hyman et al., 2014).

In this model, instead of entropy driving the system to a mixed state, the spontaneous separation into two phases (i.e. oil and vinegar) is driven by the interactions betwe en the molecules themselves which favor the formation of liquid-like droplets or condensates in the solution (Banani et al., 2017; Hyman et al., 2014). In vitro phase separation assays with purified proteins have become the standard way to investigate proteins that form membrane-less compartments. Liquid-droplet formation can be assessed by alternating the environmental conditions (such as temperature and pH) and/or by adding RNA to the purified proteins and observing the subsequent condensation. Various proteins have been purified, tested and identified for their ability to phase separate and form liquid condensates in vitro. Howe ver, in a developmental cell context, self-assembly processes must be controlled to serve a precise physiological function. Indeed cellular control by post-translational modifications to IDPs have been demonstrated in P granule formation of *C.elegans*, MEG-3 and MEG-4 (Smith et al., 2016 & Wang et al., 2014). Howe ver, cellular phase separation regulatory mechanisms in physiological and developmental contexts in vertebrates are unknown.

Here, we propose a novel paradigm for the cellular control over the condensation mechanisms by microtubules in development, in vivo. In this model, Buc granules self-assemble and phase separate in the cytoplasm of the early oocyte after the threshold concentration is reached. Subsequently, microtubule trafficking of Buc granules by dynein to the nuclear cleft of oocytes allows for the self-assembled phase-separated granules to reach an even greater concentration and further condense, leading to the formation of the mature Bb structure with solid-like properties. In addition, molecular condensates require a threshold concentration of their phase separation IDP, and therefore the MT-dependent continuous supply of Buc granules that we demonstrate inourwork likely contributes to the maintenance of the Bb forming aggregate. Further, this MT-based mechanism enables the polarized aggregation of the Bb in a single specific cellular location, which is crucial for oocyte polarization.

When awry, prion-like aggregation and molecular condensation lead to neurodegenerative disease. The regulation of Bb assembly and disassembly in the context of phase separation allows studying these mechanisms in physiological conditions, in vivo to assess how the localization of these granules to specific locations in the cell during development may be achieved. In future work, it will be extremely interesting to further explore the roles of microtubules and see if there is a need for scaffolding or mechanical support to keep that mature Bb in place and condensed.

Bb Phase Separation, the Oocyte and Female Reproduction

Phase separation may play a common and important role in preserving the quality of arrested oocytes in animals and the potential advantages of using an amyloid-like mechanism to form the Bb should continue to be explored. In mammals, the oocyte must be persevered for a long period of time. The rapid formation into a solid-like structure by forming an amyloid-like matrix, may provide the much-needed protection and storage of Bb protein and RNA. Moreover, the phase separated dynamics and amyloid-like matrix also allows for quick disassembly when needed. It is fascinating to think that Bb formation and hardening preserves the contents of the oocyte during prolonged periods of meiotic arrest. Thus, uncovering the role that phase separation plays in preserving the quality of oocytes is extremely important to developmental biology. In mammals, the Bb cannot be addressed functionally or in a live manner. In addition, almost nothing is known about the human Bb. Hence, we show here how the zebrafish oocyte provides a platform to bridge this gap and to advance our understanding of human female reproduction and health. The early stages of oocyte development studied in this work are essential for determining the number and quality of follicles for the entire female lifespan. In addition, understanding the mechanisms by which liquid-like, phase-separated granules generate and condense into harden solid-like states will lead to a greater understanding of how such organelles contribute to development and to neurodegenerative diseases.

Methods

Fish Lines and Gonad Collections

Juvenile ovaries we re collected from 5-7 we ek post-fertilization (wpf) juvenile fish: *wt*, *Tg(buc:buc-gfp-buc 3'utr*) (Riemer et al., 2016), *buc*^{p43} (Bontems et al., 2009) and *Tg(bact:EMTB-3XGFP)* (Revenu et al., 2014). Fish had a standard length (SL) measured according to (Parichy, et al., 2009) and we re consistently ~10-15mm. Ovary collection was done as in (Elkouby et al., 2016; Elkouby & Mullins 2017b). Briefly, to fix the ovaries for immunostaining, fish we re cut along the ventral midline and the lateral body wall was removed. The head and tail we re removed and the trunk pieces, with the exposed abdomen containing the ovaries, we re fixed in 4% PFA at 4°C overnight with nutation. Trunks we re then washed in PBS and ovaries we re finely dissected in cold PBS. Ovaries we re washed in PBS and then either stored in PBS at 4°C in the dark, or dehydrated and stored in 100% MeOH at -20°C in the dark.

Fluorescence Immunohistochemistry (IHC)

Adult ovaries we re collected from *wt,* transgenic and mutant fish using similar microdissection and we re imaged using a Leica S9i stereomicroscope and camera. Fluorescence immunohistochemistry (IHC) was performed as in (Elkouby et al., 2016; Elkouby & Mullins 2017b). Briefly, ovaries we re washed 2 times for 5 minutes (2x5min) in PBT (0.3% Triton X-100 in 1xPBS; if stored in MeOH, ovaries we re gradually rehydrated first), then washed 4x20min in PBT. Ovaries we re blocked for 1.5-2hrs in blocking solution (10% FBS in PBT) at room temperature, and then incubated with primary antibodies in blocking solution at 4°C overnight. Ovaries we re washed 4x20min in PBT and incubated with secondary antibodies in fresh blocking solution for 1.75hr, and we re light protected from this step onward. Ovaries we re washed 4x20min in PBT and then incubated in PBT containing DAPwe (1:1000, Molecular Probes), with or without DiOC6 (1:5000, Molecular Probes) for 50min and washed 2x5min in PBT and 2x5min in PBS. All steps we re carried out with nutation. Ovaries we re transferred into Vectashield (with DAPI, Vector Labs). Ovaries we re finally mounted betwe en two #1.5 coverslips using a 120µm spacer (Molecular Probes). Primary antibodies used we re mouse anti-GFP (1:300; Molecular Probes), rabbit anti-GFP (1:400; Molecular Probes) and rabbit anti-Buc (1:500; polyclonal antibodies against N-term, Buc peptide Yenzym Antibodies LLC). Secondary antibodies used we re Alexa Fluor 488 and 594 (1:500; Molecular Probes).

Drug Treatments

Ovaries we re dissected from *Tg(buc:buc-gfp-buc 3'utr*) or *Tg(bact:EMTB-3XGFP)* juvenile fish (6–8 wpf, SL ~10-15mm) into fresh warm HL-15 media as described in (Elkouby & Mullins, 2017b). Then HL-15 was replaced with HL-15 containing either 20µM nocodazole (Abcam #ab120630), 50µM colchicine (Sigma Aldrich #C9754), 25µM ciliobrevin (Sigma Aldrich #250401), 40µM taxol (Abcam #ab120143) or an equivalent volume of DMSO. Each drug treatment experiment contained DMSO groups and *Tg(bact:EMTB-3XGFP)* as controls. Ovaries we re incubated for 90min at 28°C in the dark. Ovaries we re then mounted for live imaging in media containing their respective drug concentration or DMSO control. Ovaries we re still healthy and viable for at least 8hrs after the 90min time point, verified by 500nM MitoTracker Mitochondria-Selective Probes (Molecular Probes #M7512). DMSO-treated ovaries always showe d normal intact microtubules.

Thioflavin (ThT) Treatment

Ovaries we re dissected from *Tg(buc:buc-gfp-buc 3'utr*) or *wt* juvenile fish (6–8 wpf, SL ~10-15mm) into fresh warm HL-15 media as described above and in (Elkouby & Mullins, 2017b). Ovaries

we re incubated with 20μM ThT (Sigma Aldrich #T3516) for 30min and then rinsed x2 in fresh warm HL-15 media before being mounted for live imaging.

Stage Specific Oocyte Isolation

Stage specific oocyte isolation was performed as described in (Elkouby & Mullins 2017b). Overall,ourlab developed a protocol to isolate stage specific oocytes from ovaries. In this protocol, oocytes are first isolated from the ovary by enzymatic digestion of connective tissue and extra-cellular matrix (ECM) components, and then separated by size using combinations of sieve sizes, cell strainers in various pore sizes (BD Falcon) and Cell-Micro-Sieves in various pore sizes 12′×12′ sheets (BioDesign Inc. of NY). The protocol was previously optimized by using a combination of three enzymes, Collagenase we (Sigma-Aldrich, #C0130), Collagenase Iwe (Sigma-Aldrich, #C6885) and Hyaluronidase (Sigma-Aldrich, #H4272), resulting in efficiently isolated intact oocytes. The digestive HL-15 mix contains (3 mg/ml Collagenase I, 3 mg/ml Collagenase II, 1.6 mg/ml Hyaluronidase, in HL-15).

L-Arginine (Pellet vs Supernatant Experiments)

Stage specific oocytes we re isolated and we re homogenized with a micropestle on ice in lysis buffer (10mM Tris (pH 7.5), 150mM NaCl, 0.5mM EDTA, 0.5% NP-40, 1X complete protease inhibitor cocktail (Roche, Mannheim)) according to (Riemer et al., 2015). After lysis, samples we re then spun down 10min at 12,000 x g at 4°C and the subsequent supernatant and pellet fractions we re isolated separately for we stern blot and/or MS analysis. L-Arginine (Sigma Aldrich #5131) concentrations of 500mM to 2.0M we re added directly to the lysis buffer when used in troubleshooting experiments.

Proteolysis and Mass Spectrometry Analysis

All MS samples we re worked up and analyzed at the Smoler Proteomics Center at the Technion (Haifa, Israel). The samples we re precipitated in 80% acetone, and washed 4 times with cold 80% acetone. The protein pellets we re dissolved in 8.5M Urea and 400mM ammonium bicarbonate and 10mM DTT. The samples we re reduced (60ºC for 30min), modified with 35.2mM iodoacetamide in 100mM ammonium bicarbonate (RT for 30min in the dark) and digested in 1.5M Urea, 66mM ammonium bicarbonate with modified trypsin (Promega), overnight at 37ºC in a 1:50 (M/M) enzyme-to-substrate ratio. An additional second trypsinization was done for 4hrs. The resulting tryptic peptides we re desalted using C18 tips (Home-made stage tips), dried and re-suspended in 0.1% Formic acid. They we re analyzed by LC-MS/MS using Q Exactive HFX mass spectrometer (Thermo) fitted with a

capillary HPLC (easy nLC 1000, Thermo). The peptides we re loaded onto a homemade capillary column (20 cm, 75micron ID) packed with Reprosil C18-Aqua (Dr. Maisch GmbH, Germany) in solvent A (0.1% formic acid in water). The peptides mixture was resolved with a (5 to 28%) linear gradient of solvent B (95% acetonitrile with 0.1% formic acid) for 120min followe d by gradient of 15min gradient of 28 to 95% and 15min at 95% acetonitrile with 0.1% formic acid in water at flow rates of 0.15µl/min. Mass spectrometry was performed in a positive mode using repetitively full MS scan followe d by high collision induces dissociation (HCD, at 25 normalized collision energy) of the 10 most dominant ions (>1 charges) selected from the first MS scan. The mass spectrometry data was analyzed using the MaxQuant software 1.5.2.8. (//www.maxquant.org) using the Andromeda search engine, searching against the *Danio rerio* proteome from the Uniprot database with mass tolerance of 4.5ppm for the precursor masses and 4.5ppm for the fragment ions. Peptide- and protein-level false discovery rates (FDRs) we re filtered to 1% using the target-decoy strategy. Protein table was filtered to eliminate the identifications from the reverse database, common contaminants and single peptide identifications. The data was quantified by label free analysis using the same software, based on extracted ion currents (XICs) of peptides enabling quantitation from each LC/MS run for each peptide identified in any of experiments. Statistical analysis of the identification and quantization results was done using Perseus 1.6.7.0 software

Western Blot

Samples we re heated to 95°C with 2X sample buffer (4X stock contains: 40% glycerol, 0.2M Tris pH 6.8, 20% ß-mercaptanol, 4% SDS and 0.005% Bromophenol Blue) for 5min prior to loading on a 4%-20% Mini-PROTEAN TGX gels (BioRad, #456-1094) and blotted using Trans-Blot Turbo Transfer Pack 0.2µm nitrocellulose (BioRad, #1704159) on the TransBlot Turbo BioRad system at 2.5A, 23V for 10min. Membranes we re blocked for 2hrs at RT in 5% milk powder before incubation overnight (o/n) at 4°C with primary rabbit anti-GFP antibody (1:1,000; Molecular Probes). Primary antibody was collected after o/n and membranes we re washed 3x for 10min in 1X TBST. Membranes we re then incubated with the secondary antibody, peroxidase-conjugated AffiniPure Goat Anti-Rabbit IgG (H+L) (Jackson ImmunoResearch, #111-035-003), for 1hr at RT. Membranes we re finally washed 5x for 5min in 1XTBST before being developed with the ECL Clarity Kit (BioRad) and imaged on ChemiDoc Imaging Systems (BioRad). Images we re analyzed on Image Lab 4.1 (BioRad).

Confocal Microscopy, Image Acquisition and Processing

Images we re acquired on a Zeiss LSM 880 confocal microscope using a 40X lens. The acquisition setting was set betwe en samples and experiments to: XY resolution=1104x1104 pixels, 12-

bit, 2x sampling averaging, pixel dwe ll time=0.59sec, zoom=0.8X, pinhole adjusted to 1.1µm of Z thickness, increments betwe en images in stacks we re 0.53µm, laser powe r and gain we re set in an antibody-dependent manner to 7-11% and 400-650, respectively, and below saturation condition. Unless otherwise noted, shown images are partial Sum Z-projection. Acquired images we re not manipulated in a non-linear manner, and only contrast/brightness we re adjusted. All figures we re made using Adobe Photoshop CC 2014 and Powe rPoint.

Confocal Live and Time-Lapse Imaging of Cultured Ovaries

Confocal live and time-lapse imaging of cultured ovaries was performed as in (Elkouby & Mullins 2017b; Mytlis & Elkouby 2021). Briefly, ovaries we re dissected from juvenile fish (5- 7wpf, SL~10-15mm) into fresh warm HL-15 media (Hanks solution containing 60% L-15 (no phenol red), Sigma-Aldrich, and 1:100 Glutamax, Invitrogen, warmed to 28°C). Ovaries we re then embedded in 0.5% low-melt agarose in HL-15 on a glass-bottom dish, and covered with warm HL-15. After the agarose polymerized, ovaries we re incubated in HL-15 at 28°C. Time-lapse images of live ovaries we re acquired using either a Zeiss LSM 880 or Nikon Ti2E spinning disc confocal microscopes, both equipped with an environmental chamber set to 28°C, and using a 40X and 60X lenses, respectively. Images we re acquired every 6 seconds for single Z section, or 18-20 seconds for Z stacks, over 5-10min.

Super-resolution Microscopy, dSTORM Imaging

we used a dSTORM system and protocol as described in (Sasson et al., 2021), which allows for imaging at approximately 20nm resolution by using photo-switchable fluorophores. All dSTORM imaging was performed on TIRF mode. Whole *Tg(bact:EMTB-3XGFP)* juvenile ovaries we re immunostained, using primary mouse anti-GFP (1:500; Molecular Probes) and rabbit anti-Buc (1:500; polyclonal antibodies against N-term, Buc peptide Yenzym Antibodies LLC). Secondaries used include anti-rabbit H+L Alexa Fluor 568 and anti-mouse H+L Alexa Fluor 488 (1:500; Life Technologies). After IHC, ovaries we re then mounted on poly-D-lysine coated coverslips (no. 1.5H, Marienfeld-superior, Lauda-Königshofen, Germany). dSTORM imaging was performed in a freshly prepared imaging buffer containing 50 mM Tris (pH 8.0), 10 mM NaCl and 10% (w/v) glucose with an oxygen-scavenging GLOX solution (0.5 mg/ml glucose oxidase (Sigma-Aldrich), 40 µg/ml catalase (Sigma-Aldrich), 10 mM cysteamine MEA (Sigma-Aldrich) and 1% β- mercaptoethanol. A Nikon Ti-E inverted microscope was used. The N-STORM Nikon system was built on TIRF illumination using a 1.49 NA 100X oil immersion objective and an ANDOR DU-897 camera. 488, 568 nm laser lines we re used for activation with cycle repeat of ~4000 cycles for each channel. Nikon NIS Element software was used for

acquisition and analysis. Analysis was also performed by ThunderSTORM (NIH ImageJ (Ovesny et al., 2014)). Images in 2D we re Gaussian fit of each localization; in the N-STORM software.

Fluorescence Recovery After Photobleaching (FRAP)

FRAP was performed on a Zeiss LSM 880 confocal microscope. In oocytes carrying Buc-GFP [*Tg(buc:buc-gfp-buc 3'utr*], an area of approximately 1/3 of the aggregate size was systematically bleached to around 20% of the original Buc-GFP intensity and then followe d recovery for 680sec (11.33min), recording every 2.5sec. These conditions we re established during initial calibration experiments. we previously observed that bleaching 1/3 of the aggregate resulted in a significant reduction in Buc-GFP signal without completely ablating all the protein in the nuclear cleft. Moreover, we observed a plateau of recovery dynamics after 680sec. Thus, to reduce any photobleaching affects all experiments had a total duration of 680sec. Regions (pre– and post-bleach) we re tracked using ROwe manager on Fiji. 10 pre-bleach frames we re recorded and after background subtraction, the average intensity was used as pre-bleach intensity. Post-bleach frames we re background subtracted and to make replicates comparable, post-bleach frame #1 of each measurement was set to 0 and corresponding pre-bleach intensity was corrected for this. Subsequently, recovery curves we re plotted and the immobile/mobile fractions we re calculated (see below) in order to determine Buc protein dynamics and turnover within individual oocytes. Mobile and Immobile fractions we re calculated according to European Advanced Light Microscopy Network (EAMNET):

Mobile fraction F_m = $(I_E - I_0) / (I_{we} - I_0)$

Immobile fraction F_i = 1 - Fm

With: I_E: End value of the recovered fluorescence intensity

I_0: first postbleach fluorescence intensity

I_I: Initial (prebleach) fluorescence intensity

Statistical Analysis

All statistical analysis and data plotting we re performed using the GraphPad Prism 7 software. Data sets we re tested with two-tailed unpaired t-test. p-values we re: *<0.01,****0.05).

References

1. Aoki, S. T., Lynch, T. R., Crittenden, S. L., Bingman, C. A., Wickens, M., & Kimble, J. (2021). *C. elegans* germ granules require both assembly and localized regulators for mRNA repression. Nature communications, 12(1), 996.
2. Banani, S.F., Lee, H.O., Hyman, A.A., and Rosen, M.K. (2017). Biomolecular condensates: organizers of cellular biochemistry. Nat. Rev. Mol. Cell Biol. 18, 285–298.
3. Blumenthal, D., Goldstien, L., Edidin, M., & Gheber, L. A. (2015). Universal Approach to FRAP Analysis of Arbitrary Bleaching Patterns. Scientific reports, 5, 11655.
4. Boeynaems, S., Alberti, S., Fawzi, N. L., Mittag, T., Polymenidou, M., Rousseau, F., Schymkowitz, J., Shorter, J., Wolozin, B., Van Den Bosch, L., Tompa, P., & Fuxreiter, M. (2018). Protein Phase Separation: A New Phase in Cell Biology. Trends in cell biology, 28(6), 420–435.
5. Boke, E., Ruer, M., Wühr, M., Coughlin, M., Lemaitre, R., Gygi, S.P., Alberti, S., Drechsel, D., Hyman, A.A., and Mitchison, T.J. (2016). Amyloid-like self-assembly of a cellular compartment. Cell 166, 637–650.
6. Boke, E., & Mitchison, T. J. (2017). The balbiani body and the concept of physiological amyloids. Cell cycle (Georgetown, Tex.), 16(2), 153–154.
7. Bontems, F., Stein, A., Marlow, F., Lyautey, J., Gupta, T., Mullins, M.C., and Dosch, R. (2009). Bucky ball organizes germ plasm assembly in zebrafish. Curr. Biol. 19, 414–422.
8. Brangwynne, C.P., Eckmann, C.R., Courson, D.S., Rybarska, A., Hoege, C., Gharakhani, J., Jülicher, F., and Hyman, A.A. (2009). Germline P granules are liquid droplets that localize by controlled dissolution/condensation. Science 324, 1729–1732.
9. Brendel, C., Rehbein, M., Kreienkamp, H. J., Buck, F., Richter, D., & Kindler, S. (2004). Characterization of Staufen 1 ribonucleoprotein complexes. The Biochemical journal, 384(Pt 2), 239–246.
10. Buchan J.R., Parker R. (2009). Eukaryotic stress granules: the ins and outs of translation. Mol. Cell 36:932–41
11. Burakov, A., Kovalenko, O., Semenova, I., Zhapparova, O., Nadezhdina, E., & Rodionov, V. (2008). Cytoplasmic dynein is involved in the retention of microtubules at the centrosome in interphase cells. Traffic (Copenhagen, Denmark), 9(4), 472–480.

12. Chang, P., Torres, J., Lewis, R.A., Mowry, K.L., Houliston, E., and King, M.L. (2004). Localization of RNAs to the mitochondrial cloud in *Xenopus* oocytes through entrapment and association with endoplasmic reticulum. Mol. Biol. Cell 15, 4669–4681.
13. Cox R.T., Spradling A.C. (2003) A Balbiani body and the fusome mediate mitochondrial inheritance during *Drosophila* oogenesis. Development. 130(8):1579-90.
14. De Smedt, V., Szöllösi, D., & Kloc, M. (2000). The balbiani body: asymmetry in the mammalian oocyte. Genesis (New York, N.Y. : 2000), 26(3), 208–212.
15. Decker C.J., Parker R. (2012). P-bodies and stress granules: possible roles in the control of translation and mRNA degradation. Cold Spring Harb. Perspect. Biol. 4:a012286
16. Delanoue, R., & Davis, I. (2005). Dynein anchors its mRNA cargo after apical transport in the *Drosophila* blastoderm embryo. Cell, 122(1), 97–106.
17. Dodson, A. E., & Kennedy, S. (2020). Phase Separation in Germ Cells and Development. Developmental cell, 55(1), 4–17.
18. Dosch R, Wagner DS, Mintzer K.A., Runke G, Wiemelt A.P., Mullins M.C. Maternal control of vertebrate development before the midblastula transition: mutants from the zebrafish I. (2004) Dev Cell. 6(6):771-80.
19. Elkouby Y.M. (2017). All in one - integrating cell polarity, meiosis, mitosis and mechanical forces in early oocyte differentiation in vertebrates. Int J Dev Biol. 61(3-4-5):179-93.
20. Elkouby, Y. M., Jamieson-Lucy, A., & Mullins, M.C. (2016). Oocyte Polarization Is Coupled to the Chromosomal Bouquet, a Conserved Polarized Nuclear Configuration in Meiosis. PLoS biology, 14(1), e1002335.
21. Elkouby, Y. M., & Mullins, M.C. (2017a). Coordination of cellular differentiation, polarity, mitosis and meiosis - New findings from early vertebrate oogenesis. Developmental biology, 430(2), 275–287.
22. Elkouby, Y.M. & Mullins, M.C. (2017b). Methods for the analysis of early oogenesis in zebrafish. Dev Biol. 430(2):310-24.
23. Escobar-Aguirre, M., Elkouby, Y.M., Mullins, M.C. (2017a) Localization in oogenesis of maternal regulators of embryonic development. Adv. Exp. Med. Biol. 953, 173–207.
24. Escobar-Aguirre, M., Zhang, H., Jamieson-Lucy, A., & Mullins, M. C. (2017b). Microtubule-actin crosslinking factor 1 (Macf1) domain function in Balbiani body dissociation and nuclear positioning. PLoS genetics, *13*(9), e1006983.
25. Folkmann, A. W., Putnam, A., Lee, C. F., & Seydoux, G. (2021). Regulation of biomolecular condensates by interfacial protein clusters. Science (New York, N.Y.), 373(6560), 1218–1224.

26. Frey S., Gorlich D. (2007). A saturated FG-repeat hydrogel can reproduce the permeability properties of nuclear pore complexes. Cell 130:512–23
27. Giakoumakis, N. N., Rapsomaniki, M. A., & Lygerou, Z. (2017). Analysis of Protein Kinetics Using Fluorescence Recovery After Photobleaching (FRAP). Methods in molecular biology (Clifton, N.J.), 1563, 243–267.
28. Gong, C., & Maquat, L. E. (2011). lncRNAs transactivate STAU1-mediated mRNA decay by duplexing with 3' UTRs via Alu elements. Nature, 470(7333), 284–288.
29. Gross-Thebing, T., & Raz, E. (2020). Dead end and Detour: The function of the RNA-binding protein Dnd in posttranscriptional regulation in the germline. Current topics in developmental biology, 140, 181–208.
30. Guo L. & Shorter J. (2015); It's Raining Liquids: RNA Tunes Viscoelasticity and Dynamics of Membraneless Organelles. Mol Cell. 60(2):189-92.
31. Gupta, T., Marlow, F. L., Ferriola, D., Mackiewicz, K., Dapprich, J., Monos, D., & Mullins, M. C. (2010). Microtubule actin crosslinking factor 1 regulates the Balbiani body and animal-vegetal polarity of the zebrafish oocyte. PLoS genetics, 6(8), e1001073.
32. Hanson, K. K., & Mair, G. R. (2014). Stress granules and Plasmodium liver stage infection. Biology open, 3(1), 103–107.
33. Heim, A. E., Hartung, O., Rothhämel, S., Ferreira, E., Jenny, A., & Marlow, F. L. (2014). Oocyte polarity requires a Bucky ball-dependent feedback amplification loop. Development (Cambridge, England), 141(4), 842–854.
34. Hennig, S., Kong, G., Mannen, T., Sadowska, A., Kobelke, S., Blythe, A., Knott, G. J., Iyer, K. S., Ho, D., Newcombe, E. A., Hosoki, K., Goshima, N., Kawaguchi, T., Hatters, D., Trinkle-Mulcahy, L., Hirose, T., Bond, C. S., & Fox, A. H. (2015). Prion-like domains in RNA binding proteins are essential for building subnuclear paraspeckles. *The Journal of cell biology*, *210*(4), 529–539.
35. Hertig A.T. (1968) The primary human oocyte: some observations on the fine structure of Balbiani's vitelline body and the origin of the annulate lamellae. Am J Anat. 122(1):107-37.
36. Houtsmuller A. B. (2005). Fluorescence recovery after photobleaching: application to nuclear proteins. Advances in biochemical engineering/biotechnology, 95, 177–199. https://doi.org/10.1007/b102214
37. Hyman, A.A., Weber, C.A., and Jülicher, F. (2014). Liquid-liquid phase separation in biology. Annu. Rev. Cell Dev. Biol. 30, 39–58.

38. Jamieson-Lucy, A., & Mullins, M. C. (2019). The vertebrate Balbiani body, germ plasm, and oocyte polarity. Current topics in developmental biology, 135, 1–34.
39. Jeske, M., Bordi, M., Glatt, S., Müller, S., Rybin, V., Müller, C.W., and Ephrussi, A. (2015). The crystal structure of the *Drosophila* germline inducer Oskar identifies two domains with distinct vasa helicase- and RNA-binding activities. Cell Rep. 12, 587–598.
40. Kang, M., Andreani, M., & Kenworthy, A. K. (2015). Validation of Normalizations, Scaling, and Photofading Corrections for FRAP Data Analysis. PloS one, 10(5), e0127966. https://doi.org/10.1371/journal.pone.0127966
41. Kaufman O.H., Lee K., Martin M., Rothhamel S., Marlow F.L. (2018). rbpms2 functions in Balbiani body architecture and ovary fate. PLoS Genet. 14(7):e1007489.
42. Kistler, K.E., Trcek, T., Hurd, T.R., Chen, R., Liang, F.X., Sall, J., Kato, M., and Lehmann, R. (2018). Phase transitioned nuclear Oskar promotes cell division of *Drosophila* primordial germ cells. eLife 7, e37949.
43. Kloc, M., Bilinski, S., and Etkin, L.D. (2004). The Balbiani body and germ cell determinants: 150 years later. Curr. Top. Dev. Biol. 59, 1–36.
44. Krammer, C., Schätzl, H. M., & Vorberg, I. (2009). Prion-like propagation of cytosolic protein aggregates: insights from cell culture models. *Prion*, *3*(4), 206–212. https://doi.org/10.4161/pri.3.4.10013
45. Langdon Y.G., Mullins M.C. (2011) Maternal and zygotic control of zebrafish dorsoventral axial patterning. Annu Rev Genet. 45:357-77.
46. Lei L., Spradling A.C. (2016) Mouse oocytes differentiate through organelle enrichment from sister cyst germ cells. Science. 352(6281):95-9.
47. Li, P., Banjade, S., Cheng, H. C., Kim, S., Chen, B., Guo, L., Llaguno, M., Hollingsworth, J. V., King, D. S., Banani, S. F., Russo, P. S., Jiang, Q. X., Nixon, B. T., & Rosen, M. K. (2012). Phase transitions in the assembly of multivalent signaling proteins. Nature, 483(7389), 336–340.
48. Luo, Y., Na, Z., & Slavoff, S. A. (2018). P-Bodies: Composition, Properties, and Functions. Biochemistry, 57(17), 2424–2431.
49. Mahen R., Venkitaraman A.R. (2012). Pattern formation in centrosome assembly. Curr. Opin. Cell Biol. 24:14–23
50. Marlow F.L., Mullins M.C. (2008). Bucky ball functions in Balbiani body assembly and animal-vegetal polarity in the oocyte and follicle cell layer in zebrafish. Developmental Biology. 321(1):40-50.

51. Marnik, E.A., Fuqua, J.H., Sharp, C.S., Rochester, J.D., Xu, E.L., Holbrook, S.E., and Updike, D.L. (2019). Germline maintenance through the multifaceted activities of GLH/vasa in *Caenorhabditis elegans* P Granules. Genetics 213, 923–939.
52. Mytlis A. & Elkouby YM. Live and Time-lapse Imaging of Early Oogenesis and Meiotic Chromosomal Dynamics in Cultured Juvenile Zebrafish Ovaries. (2021) Methods Mol Biol. 2021;2218:137-155.
53. Mytlis, A., Kumar, V., Tao, Q., Deis, R., Levy, K., Masek, M., Eitan, H., Nather, F., Shawahny, A., Bachmann-Gagescu, R., Roy, S., Elkouby, Y. M. (2021). Ciliary control of meiotic chromosomal pairing mechanics and germ cell morphogenesis. biorxiv, 2021.2002.2008.430249.
54. Nott, T.J., Petsalaki, E., Farber, P., Jervis, D., Fussner, E., Plochowietz, A., Craggs, T.D., Bazett-Jones, D.P., Pawson, T., Forman-Kay, J.D., and Baldwin, A.J. (2015). Phase transition of a disordered nuage protein generates environ- mentally responsive membraneless organelles. Mol. Cell 57, 936–947.
55. Ovesný, M., Křížek, P., Borkovec, J., Svindrych, Z., & Hagen, G. M. (2014). ThunderSTORM: a comprehensive ImageJ plug-in for PALM and STORM data analysis and super-resolution imaging. Bioinformatics (Oxford, England), 30(16), 2389–2390.
56. Parichy, D. M., Elizondo, M. R., Mills, M. G., Gordon, T. N., & Engeszer, R. E. (2009). Normal table of postembryonic zebrafish development: staging by externally visible anatomy of the living fish. Developmental dynamics: an official publication of the American Association of Anatomists, 238(12), 2975–3015.
57. Pepling M.E., Wilhelm J.E., O'Hara A.L., Gephardt G.W., Spradling A.C. (2007) Mouse oocytes within germ cell cysts and primordial follicles contain a Balbiani body. Proc Natl Acad Sci U S A.104(1):187-92.
58. Putnam, A., Cassani, M., Smith, J., & Seydoux, G. (2019). A gel phase promotes condensation of liquid P granules in Caenorhabditis elegans embryos. Nature structural & molecular biology, 26(3), 220–226.
59. Riemer, S., Bontems, F., Krishnakumar, P., Gömann, J., & Dosch, R. (2015). A functional Bucky ball-GFP transgene visualizes germ plasm in living zebrafish. Gene expression pattern: GEP, 18(1-2), 44–52.
60. Revenu, C., Streichan, S., Donà, E., Lecaudey, V., Hufnagel, L., Gilmour, D. (2014) Quantitative cell polarity imaging defines leader-to-followe r transitions during collective migration and the key role of microtubule-dependent adherens junction formation. Development (Cambridge, England). 141:1282-91

61. Rog, O., Köhler, S., & Dernburg, A. F. (2017). The synaptonemal complex has liquid crystalline properties and spatially regulates meiotic recombination factors. eLife, 6, e21455.
62. Rong, Y., Ji, S. Y., Zhu, Y. Z., Wu, Y. W., Shen, L., & Fan, H. Y. (2019). ZAR1 and ZAR2 are required for oocyte meiotic maturation by regulating the maternal transcriptome and mRNA translational activation. Nucleic acids research, 47(21), 11387–11402.
63. Roovers, E.F., Kaaij, L.J.T., Redl, S., Bronkhorst, A.W., Wiebrands, K., de Jesus Domingues, A.M., Huang, H.Y., Han, C.T., Riemer, S., Dosch, R., et al. (2018). Tdrd6a regulates the aggregation of Buc into functional subcellular compartments that drive germ cell specification. Dev. Cell 46, 285–301.e9.
64. Sasson, E., Anzi, S., Bell, B., Yakovian, O., Zorsky, M., Deutsch, U., Engelhardt, B., Sherman, E., Vatine, G. D., Dzikowski, R., Ben-Zvi, A. (2021). Nano-scale Architecture of Blood-Brain Barrier Tight-Junctions. bioRxiv 2021.08.12.456150.
65. Schisa J. A. (2012). New insights into the regulation of RNP granule assembly in oocytes. International review of cell and molecular biology, 295, 233–289.
66. Scialò, C., De Cecco, E., Manganotti, P., & Legname, G. (2019). Prion and Prion-Like Protein Strains: Deciphering the Molecular Basis of Heterogeneity in Neurodegeneration. Viruses, 11(3), 261.
67. Selman K., Wallace R.A., Sarka A., Qi X.P. (1993) Stages of Oocyte Development in the Zebrafish, Brachydanio- Rerio. Journal of Morphology. 218(2):203-24.
68. Seydoux G. (2018). The P Granules of *C. elegans*: A Genetic Model for the Study of RNA-Protein Condensates. Journal of molecular biology, 430(23), 4702–4710.
69. Shin, Y., and Brangwynne, C.P. (2017). Liquid phase condensation in cell physiology and disease. Science 357, eaaf4382.
70. Smith, J., Calidas, D., Schmidt, H., Lu, T., Rasoloson, D., & Seydoux, G. (2016). Spatial patterning of P granules by RNA-induced phase separation of the intrinsically-disordered protein MEG-3. *eLife*, *5*, e21337.
71. Spike, C.A., Bader, J., Reinke, V., and Strome, S. (2008). DEPS-1 promotes P- granule assembly and RNA interference in *C. elegans* germ cells. Development 135, 983–993.
72. So, C., Cheng, S., & Schuh, M. (2021). Phase Separation during Germline Development. Trends in cell biology, 31(4), 254–268.
73. Tian, S., Curnutte, H. A., & Trcek, T. (2020). RNA Granules: A View from the RNA Perspective. Molecules (Basel, Switzerland), 25(14), 3130.

74. Trcek, T., Grosch, M., York, A., Shroff, H., Lionnet, T., and Lehmann, R. (2015). *Drosophila* germ granules are structured and contain homotypic mRNA clusters. Nat. Commun. 6, 7962.
75. Wang, J.T., Smith, J., Chen, B.C., Schmidt, H., Rasoloson, D., Paix, A., Lambrus, B.G., Calidas, D., Betzig, E., and Seydoux, G. (2014). Regulation of RNA granule dynamics by phosphorylation of serine-rich, intrinsically disordered proteins in *C. elegans*. eLife 3, e04591.
76. Westerfield, M. (2000). The zebrafish book. A guide for the laboratory use of zebrafish (*Danio rerio*). 4th ed., Univ. of Oregon Press, Eugene.
77. Woodruff, J.B., Hyman, A.A., and Boke, E. (2018). Organization and function of non-dynamic biomolecular condensates. Trends Biochem. Sci. 43, 81–94.
78. Xue, C., Lin, T. Y., Chang, D., & Guo, Z. (2017). Thioflavin T as an amyloid dye: fibril quantification, optimal concentration and effect on aggregation. Royal Society open science, 4(1), 160696.
79. Yang, J., Aguero, T., & King, M. L. (2015). The *Xenopus* Maternal-to-Zygotic Transition from the Perspective of the Germline. Current topics in developmental biology, 113, 271–303.
80. Zhang, H., Elbaum-Garfinkle, S., Langdon, E. M., Taylor, N., Occhipinti, P., Bridges, A. A., Brangwynne, C. P., & Gladfelter, A. S. (2015). RNA Controls PolyQ Protein Phase Transitions. Molecular cell, 60(2), 220–230.

Acknowledgments

We thank Roland Dosch for the Tg(buc:Buc-GFP) line and Mary Mullins for the Buc antibody. We are grateful to Ayal Ben-Zvi for his help with super-resolution microscopy. We thank the Smoler Proteomics Center of The Technion-Israel Institute of Technology for their help with MS experiments.

Funding

This work was funded by ISF grant #558/19.

Competing interests: Authors declare that they have no competing interests.